2004

Effects of submergence and test startup conditions on local scour by plane turbulent wall jets.

Niranjan P. Deshpande
University of Windsor

NOTE TO USERS

EFFECTS OF SUBMERGENCE AND TEST STARTUP CONDITIONS ON LOCAL SCOUR BY PLANE TURBULENT WALL JETS

by

Niranjan P Deshpande

A Thesis
Submitted to the Faculty of Graduate Studies and Research
through the Department of Civil and Environmental Engineering
in Partial Fulfillment of the Requirements for
the Degree of Master of Applied Science at the
University of Windsor

Windsor, Ontario, Canada

2004

Your file Votre référence
ISBN: 0-612-96401-9
Our file Notre référence
ISBN: 0-612-96401-9

ABSTRACT

Experiments were carried out to study the interaction of plane turbulent wall jets with cohesionless soils during scour. The jet of water having a constant mean velocity of 1.16 m/s and thickness of 25.4 mm at the nozzle exit was set to initially flow tangentially along the sand bed with a median grain size of 2.15 mm. Both scour profile measurements and velocity measurements were obtained for a range of submergences, defined by the ratio of the tailwater depth to the nozzle opening. The results confirm the presence of two distinct types of flow fields, one that occurs at lower submergences and the other at higher submergences of the jet. At low submergences, laser Doppler anemometer measurements indicate that the jet flow is initially close to the bed and then flicks towards the water surface, whereas at the higher submergences, no such flicking movement was noticed. At higher submergences, however, the jet impingement point on the sand bed was highly unsteady. Low pass filtering of the velocity data give further details of these processes. It is seen that the movement of the impingement point for high submergences is more rapid with decreasing submergence.

Furthermore, variations in scour and velocity profiles were noted in the mound region across the flume cross-section, and were found to be dependent on the level of submergence. In an effort to clarify some of the differences noted in the scour characteristics in earlier studies, the test startup conditions were varied. This includes an instantaneous, a gradual and a stepwise startup condition. The velocity measurements indicate that the flow gradually evolves to a state that is independent of the startup conditions. However, the scour profiles appear to be dependent on the startup conditions for a longer period of time.

To My Father and My Mother

ACKNOWLEDGEMENTS

I would like to express my sincere gratitude and profound appreciation to my supervisors, Dr. Ram Balachandar and Dr. Kerry Mazurek for their patience, invaluable supervision, guidance, thoughtful insights and so generously taking out your times to discuss varied aspects of this research. I would like to acknowledge the financial assistance and compassionate support from my supervisors that always motivated me and helped me to put behind all worries and difficulties. I consider it a matter of great privilege and a rare opportunity to work under their supervision.

Gratitude is also expressed to Dr. Nihar Biswas and Dr. David Ting, the members of the examination committee, for their helpful comments, suggestions and encouragement.

I wish to extend my sincere thanks to Mr. Richard Clark and Mr. Lucien Pop for their prompt help and support in building and maintaining the experimental setup for this study. Special thanks to my friends and fellow graduate students for their encouragement and their interest shown in this study.

Lastly, my thanks also go to my mother and my brother for their continued support and advice that have always helped me to put things in perspective and remain focused. Thank you very much for always being there.

TABLE OF CONTENTS

LIST OF TABLES

LIST OF FIGURES

LIST OF SYMBOLS

b_o	Thickness of nozzle opening
d	Characteristic depth
D_{50}	Median size of bed material
D_i	Bed material diameter, i% of which is finer by weight
F_o	Densimetric Froude number
F_r	Flow Froude number
g	Acceleration due to gravity
h	Mound height
Re	Reynolds number
t	time
u_m	mean velocity
u_{rms}	Root mean square velocity
U	Flow velocity
U_m	Maximum velocity
U_o	Velocity of the jet at the nozzle (origin)
V	Instantaneous velocity
x	Distance from the nozzle
x_d	Distance of maximum mound height from the nozzle
x_m	Distance of maximum scour depth from the nozzle
x_o	Length of the scour hole
y_t	Tailwater depth
δ	Boundary layer thickness

δ_1 Vertical length scale where $U = 0.5U_m$

δ_2 Depth of forward flow

Δ Maximum mound height

$\Delta\rho$ Difference between mass densities of the particle and eroding fluid

ε Scour depth

ε_m Maximum scour depth

ν Kinematic viscosity of the eroding fluid

ρ Mass density of water

σ_g Geometric standard deviation of the bed material

CHAPTER 1: INTRODUCTION

1.1 Introduction

Scour occurs naturally as part of morphologic changes of rivers and streams caused by the flow of water and also as the result of man-made structures. Scour can be defined as the enlargement of a flow section by the removal of material composing the boundary through the action of fluid in motion (Laursen 1952). The prediction of scour in the vicinity of hydraulic structures such as spillways, weirs, drops, and culvert and pipe outlets is complicated by the various flow patterns that occur due to the interaction with the moveable boundary. Even in seemingly simple flow fields, the evolution of scour and the flow interaction with the sand particles can be complex. In order to gain an insight into the more detailed features of scour, researchers have had to resort to experimentation. Some of the first of these studies include that of Rouse (1939), Laursen (1952) and Tarapore (1956).

Scour below hydraulic structures and outlets is typically caused by turbulent water jets, where the jets are flows of generally high velocities as compared to the surrounding fluid (Rajaratnam, 1976). Experience has shown that scouring can progressively undermine the foundation of a structure and cause the structure to fail (Breusers and Raudkivi, 1991). It is thus important for hydraulic engineers to understand the mechanism of scour and find ways to guide and control the process in order to minimize the risk of failure.

Studies of scour by jets have included jets in many different configurations. These include horizontal and vertical jets, two and three-dimensional jets, submerged or free jets, and jets with various boundary configurations (Breusers and Raudkivi, 1991).

Furthermore, jets can be classified as plane and circular jets, free and wall jets, and offset and impinging jets. The focus of this thesis is to study the scour produced by flows that behave similar to plane turbulent wall jets. The plane wall jet is defined as a rectangular jet (having a large aspect ratio) that initially flows tangentially along a boundary surrounded by stationary (or moving) fluid (Rajaratnam, 1976). The classical wall jet is very deeply submerged. Flows under a sluice gate, at outlets with rectangular cross sections, or a hydraulic jump in a rectangular channel all can behave similarly to plane wall jets (Rajaratnam, 1965a), although the submergence of the flow would be likely less than the classical wall jet case (Wu and Rajaratnam, 1995).

Various researchers have conducted experiments on scour caused by plane wall jets in both cohesive and cohesionless soils. It is important to note that the present study is concerned with scour in cohesionless soils only. Most previous studies have concentrated on the erosion or scour of cohesionless soils by deeply submerged plane turbulent wall jets (Laursen, 1952; Tarapore, 1956; Rajaratnam, 1981; Aderibigbe and Rajaratnam, 1998), although there also have been some which have considered submergence effects (Rajaratnam and Macdougall, 1983; Ali and Lim, 1986; Johnston, 1990; Mohamed, 1990; Mohamed and McCorquodale, 1992; Chatterjee et al, 1994; Balachandar and Kells, 1997; Balachandar et al, 2000; and Kells et al, 2001). Laursen (1952) found that for deep submergences, where submergence is defined as the ratio of y_t/b_o (y_t being the tailwater depth and b_o, the jet opening or thickness), the process of scour development is well-defined and that the scour profile consisted of a scour hole and a mound. Rouse (1939) had concluded that the removal of material continued as an exponential function of the time, with only the fixed boundaries governing the ultimate

limit of excavation. However, Laursen (1952) challenged this concept, reasoning that after the scour hole is sufficiently enlarged, the velocities would not be large enough to carry any more sediment. Later, Tarapore (1956) showed that, after some time, the scour hole did reach a stable or equilibrium state, which has frequently been called the asymptotic state of scour. The development of scour for deep submergences varies linearly with the logarithm of time up to some time, until scour nears the state of equilibrium or asymptotic condition, when the scour hole size becomes approximately constant with time (Tarapore, 1956; Rajaratnam, 1981).

For scour with lower submergences, this well-defined asymptotic state may or may not be observed (Johnston et al, 1987; Johnston, 1990; Balachandar et al, 2000; Ahsan and Mazurek, 2003). The development of scour mechanism and its associated flow pattern can be unstable and complex in nature depending on the range of submergence (Johnston, 1990; Ahsan and Mazurek, 2003). For example, the flow in the vicinity of the gate observed by Rajaratnam and Macdougall (1983) fluctuated continuously from a surface jet to a hydraulic jump to a submerged hydraulic jump and back to a surface jet with minimum tailwater. The proximity of the bed and the free surface has a considerable influence on the nearfield flow pattern that can promote the flicking of the jet from one boundary to another (Johnston, 1990). This interaction can thus strongly affect the scour hole development. This unstable jet phenomenon was later observed by Balachandar and Kells (1997), Balachandar et al (2000) and Kells et al (2001) who reported occurrence of two cyclically alternating flow fields and the presence of a secondary mound that was observed to form just downstream of the scour hole for lower submergences. It appears that the depth of flow available above the mound apex plays the most significant role in

causing the instability, which can either be short or long-term in nature (Ahsan, 2003). A more detailed discussion of the phenomenon of scour by plane wall jets is provided in Chapter 2.

It is thus clear that even for a simple flow emanating from nozzles (or sluice gates), the flow and the corresponding scour pattern can become complex due to various influences. It should be remarked that Aderibigbe and Rajaratnam (1998) observed a deeper dynamic maximum scour depth and a shallower dynamic maximum scour depth for deep submergences. Dynamic scour refers to the case when the water flow is kept running during the observation of the scour development. Further, the commencement of the flow or the test startup conditions are quite varied in the studies noted above. In some preliminary experiments in studying the effects of submergence on scour by plane wall jets using a similar setup to that of Ahsan (2003), there was a large amount of variation across the width of the scour hole. Most of the earlier studies did not report this variation. Due to lack of understanding of the effect of test startup conditions and uncertainty of jet behavior in the scour hole, there is a need for closer investigation of different flow regimes in scour by plane jets, and the scour produced by these regimes.

1.2 Objectives of the Study

The objectives of this study are:

(1) To study the characteristics of different regimes of flow behavior for a range of submergence and the scour produced by these regimes; and

(2) To investigate the effect of test startup conditions on plane turbulent wall jet behavior and the resulting scour profiles.

1.3 Organization of the Thesis

This thesis is divided into five chapters. Chapter 2 includes a review of previous studies on scour by plane wall jets in cohesionless materials. Chapter 3 discusses the experimental setup, measurements, and testing program for the present study. Chapter 4 presents the observations, results and analysis of the experiments. Finally, conclusions and recommendations are made in Chapter 5.

CHAPTER 2: LITERATURE REVIEW

2.1 Introduction

In this chapter, basic features of a plane turbulent wall jet are discussed. This is followed by a review of previous studies on scour of cohesionless soils by plane turbulent wall jets. These studies are divided into those with high and low submergences of the jet.

2.2 Plane Turbulent Wall Jets

Since the turbulent wall jet is the scouring agent investigated in the present study, the general characteristics of the classical wall jet are introduced. A plane turbulent wall jet, as defined by Rajaratnam (1976), is a jet of thickness b_o and uniform velocity U_o issuing from a rectangular slot tangentially to a flat plate surrounded by stationary (or moving) fluid (Figure 2-1). The classical wall jet is a case when the plane turbulent wall jet issues into the same stationary fluid of semi-finite extent on a rigid boundary (Karim and Ali, 2000). As soon as the jet leaves the slot or the nozzle, due to the velocity discontinuity, a shear layer develops on the fluid side while a boundary layer develops on the wall side. The section where the boundary layer meets the penetrating shear layer, the potential core of the jet ends and beyond which the flow is said to be fully developed. Extensive studies of experimental investigations on the plane turbulent wall jets have been carried out and can be found in the literature (Rajaratnam, 1976; Karlsson et al, 1992; Wygnanski et al, 1992; Hussein et al, 1994; Venas et al, 1999; Tachie, 2001; and Ead and Rajaratnam, 2002). Most of the studies have shown that at any x-station the axial velocity u increases from zero at the wall to reach its

maximum value u_m at a distance of $y = \delta$ and then decreases to reach zero at large y. The region from the wall ($y = 0$) to the region where $y = \delta$ is called the boundary layer and the region above this is known as the free mixing region. Further, the observations of the variation of the axial velocity u(y) with y, at different x-stations, have shown that the velocity profiles have same shapes.

There are four possible flow regimes in a channel depending on the tailwater conditions, viz., a supercritical stream, hydraulic jump, submerged hydraulic jump, and deeply submerged jump. A supercritical stream is defined as a flow where the flow Froude number, $F_r > 1$ ($F_r = U_o/\sqrt{g y_o}$, where g = acceleration due to gravity and y_o is the initial depth of flow entering the channel). If the tailwater depth (y_t) is less than the subcritical ($Fr < 1$) sequent depth (y_2) this supercritical stream will continue along the channel. The initial flow depth starts increasing further downstream of the channel due to the friction on the bed and will eventually form a hydraulic jump when y_t equals to y_2. The hydraulic jump is a rapid transition from supercritical to subcritical flow. In this case the tailwater depth y_t is equal to the subcritical sequent depth y_2, given by the Belanger equation

$$\frac{y_2}{y_1} = \frac{1}{2}\left(\sqrt{1+8F_r^{\,2}} - 1\right) \tag{2.1}$$

where, F_r = supercritical Froude number as defined earlier. If the tailwater depth is less than y_2, the jump would form somewhere downstream and is referred to as a repelled jump. If y_t is greater than y_2, a submerged jump is formed at the gate (or nozzle). A submerged jump is characterized by the supercritical Froude number F_r and the submergence factor S, defined as $(y_t - y_2)/y_2$ (Rajaratnam, 1965a).

Rajaratnam (1965a) suggested that the deeply submerged hydraulic jump could be treated as a plane wall jet under an adverse pressure gradient with backward flow on top. The adverse pressure gradient is fixed by the supercritical Froude number, F_r and the submergence factor, S. According to Wu and Rajaratnam (1995), in case of certain submerged jumps, the decay of the velocity scale is wall-jet-like (or WJL) and in others, it is free-jump-like (or FJL). They defined two parameters viz., S^* and $S^\#$ and found that for any given value of F_r, for S greater than S*, the decay will be WJL whereas for S smaller than S*, the decay will be FJL. Also, a classical wall jet (W) decay was seen if S was greater than $S^\#$.

2.3 Scour by Plane Turbulent Wall Jets

This section discusses the general features of scour in cohesionless soils by plane turbulent wall jets. Firstly, to understand the mechanism of scour by water jets, consider a turbulent jet issuing from a two-dimensional or a three-dimensional nozzle. This jet possesses tremendous scouring potential created by the high incoming velocity resulting in sediments immediately being dislodged from the initial flat erodible bed, lifted and held in suspension due to counterclockwise eddies, and then transported downstream at a rapid rate. For a small time period, the vertical dimensions of the scour hole increase at a faster rate than the horizontal dimensions and the bed material is transported mainly as bed loads (Karim and Ali, 2000). This entrainment, transportation and deposition of sediments depend not only on the hydraulic characteristics of the flow but also as much on the properties of the sediments. The scouring mechanism involves a combination of two relative motions: that of the flow field relative to the boundary, and that of the bed material relative to the overlying flowing fluid (Karim and Ali, 2000).

Studies on scour in cohesionless soils by plane turbulent wall jets have broadly been classified into deeply submerged and shallow submergence cases. There has not been any established demarcation between deep (or high) and shallow (or low) submergences. However, Ali and Lim (1986) suggested that the effect of tailwater on scour hole development becomes insignificant for $y_t/b_o > 16$.

2.3.1 High submergence

For higher submergences, the process of scour development occurs in a well-defined manner and the scour profile typically consists of a scour hole and a mound as shown in Figure 2-2 (Laursen, 1952). The depth of water increases as the scour hole gradually enlarges with time. Hence from the principle of continuity, the mean flow velocity reduces as a result of the expanding cross sectional area (Ali and Lim, 1986). Thus it has been observed that for two-dimensional jets, the local velocity near the scoured bed decreases as the depth of the scour hole increases resulting in a decrease in the rate of erosion as time progresses (Ali and Lim, 1986; Karim and Ali, 2000). However, beyond the deepest part of the scour hole, the flow begins to converge with a corresponding increase in velocity (Ali and Lim, 1986). For larger time periods, the bed velocity eventually reduces to a certain "critical" value as a result of which the flow (near the bed) becomes incapable of removing further bed material from the scour area (Karim and Ali, 2000). At this point, the scour geometry is said to have achieved its "equilibrium" or "asymptotic" condition as observed in studies by Tarapore (1956), Chatterjee and Ghosh (1980), Rajaratnam (1981), and Ahsan (2003).

Tarapore (1956) suggested that the time taken to reach an equilibrium state and the size of the scour hole are functions of the sediment properties, the velocity and

thickness of the jet, and the depth of the tailwater. Tarapore (1956) also showed that the limiting size of the scour hole increases as the square of the velocity and decreases with increasing critical tractive force of the sediment. Further, the time taken to achieve a certain scour in inversely proportional to the fourth power of the velocity and hence a higher velocity would tend to achieve equilibrium earlier than a lower velocity. According to Tarapore (1956), the physical picture of a submerged jet issuing into a high tailwater may be summarized in three steps, namely, an early turbulent pattern where the length of the scour hole is more or less random, advanced transportation of bed material where length of scour hole is directly proportional to the logarithm of time and the velocities at the boundaries of the hole becoming low enough that an asymptotic state is reached.

Further, the development of scour profile is related to the densimetric Froude number (F_o) (defined as $F_o = U_o / \sqrt{gD_{50}(S-1)}$, where U_o is the velocity of the jet at the nozzle, g is the acceleration due to gravity and S is the specific gravity of the sediment), which is a measure of the ratio of the tractive force acting on the sand grain to the submerged specific weight of the grain (Rajaratnam, 1981; Ali and Neyshaboury, 1991). For deeper submergence, the flow shows a regular behavior without the presence of instability and is called a "stable" flow (Ahsan, 2003). According to Ahsan (2003), the point of flow impingement confines itself within the scour hole for stable scour profiles. However, Aderibigbe and Rajaratnam (1998) observed that (especially for $F_o \geq 5$) the jet issuing from a nozzle for deep submergences oscillates between a position along the bed and a position in the horizontal direction.

For a range of submergence (y_t/b_o) from 12 to 60, Aderibigbe and Rajaratnam (1998) observed that when the jet was horizontal, it would entrain and drag the fluid beneath it resulting in a low pressure that would cause the jet to flow along the bed. This resulted in strong erosion of the bed and transportation of sediments over the dune. The maximum depth of scour observed during this process was termed as the deeper dynamic maximum scour depth ε'_{md}. After some time, a reverse flow that occurred led to an increase in the pressure underneath the jet causing it to rise toward the horizontal position. The rising jet caused the impingement area to shift further downstream resulting in the piled deposits to slump back into the scour hole. The maximum depth at this point was referred to as the shallower dynamic maximum scour depth ε'_{ms}. According to Aderibigbe and Rajaratnam (1998), this process was observed to continuously repeat itself.

2.3.2 Low submergence

In low submergences, unstable flow is an expected phenomenon along with a possibility of digging and filling cycles of the scour hole with variation of the jet direction (Johnston, 1990; Balachandar and Kells, 1997; Balachandar et al., 2000; Kells et al., 2001; Ahsan, 2003; Ahsan and Mazurek, 2003). Johnston (1990) carried out experiments at varying submergence (y_t/b_o=0.52-4.03) by keeping the jet opening, bed roughness and F_o constant. Johnston (1990) observed that at the highest tailwater depth tested (y_t/b_o=4.03) the jet mainstream clearly attached itself to the erodible bed and very quickly developed a scour hole with a ridge positioned just downstream of the hole thus calling it a 'bed-jet' regime. At the lowest tailwater depth (y_t/b_o=0.52) a different pattern developed where the scourhole was longer and shallower in the streamwise

direction as compared to the bed jet case, also, the ridge was less pronounced and tended to move downstream fairly quickly. The main reason for this difference was the jet being attached to the free surface and not the erodible bed. This regime was termed as the 'surface jet' regime. The most interesting observations were made at the intermediate tailwater depths where the jet flicked from the bed to the surface and back to the bed with change in scour hole developments. Johnston (1990) called this regime as the 'bed-surface' regime. He further comments that the change in the value of the slot offset (P/d_o), where P is the vertical distance from the jet centerline to bed, with increasing scour depth is mainly responsible for this flicking of the jet between boundaries and the cause for the different scourhole regimes. The flicking of the jet from one boundary to another also seems dependent on the relative influences of the two boundaries. Where the influence of one of the boundaries (bed or surface) is very strong the flick to the other boundary is for a very short period (few seconds) and is fairly random (Johnston, 1990) The results of Johnston's (1990) experiments also show that for both the bed and surface regimes the scourhole depth increases with an increase in time, the increase being more pronounced in the bed case. This trend was not apparent in the bed-surface regime where the scourhole depth remains relatively constant (Johnston, 1990).

Balachandar and Kells (1997), Balachandar et al (2000) and Kells et al (2001) observed the occurrence of two cyclically alternating flow fields and the presence of the mound that was observed to form just downstream of location of the maximum depth of scour for lower submergence (y_t/b_o=4.0-8.9). The first flow field was characterized by the presence of a strong erosion process (digging), with the predominant movement of

the bed material being in the downstream direction, which occurred for a short period of time (10-25 s). The second flow field was accompanied by the slow movement of bed material in the upstream direction that resulted in the refilling of the previously eroded portion of the bed. The refilling occurred over a relatively longer period of time (100-1000 s). The refilling period continued until the sand particles moving upstream reached the end of the protected bed and thereafter the digging state commenced once again. The water surface was also observed to change simultaneously with respect to the changes in the bed profile. A significant wave action of the water surface was noted during the refilling phase when the jet is directed towards the free surface (Balachandar and Kells, 1997; Balachandar et al., 2000; Kells et al., 2001). Further, Balachandar and Kells (1997), Balachandar et al (2000) and Kells et al (2001) report that the state of equilibrium for shallow submergences is never reached, whereas some studies with shallow submergences (Chatterjee and Ghosh, 1980; Rajaratnam and Macdougall, 1983; Chatterjee et al., 1994) have observed this state of equilibrium.

This provides for further detailed investigation of scour hole development for low submergences. However, the instability can also be early and short-term or long-term in nature with the depth of flow available above the mound apex being an important factor in causing the instability (Ahsan, 2003). Finally, the scour profile development in shallow submergences has also been found to be dependant on F_o (Rajaratnam and Macdougall, 1983; Ahsan, 2003).

Mohamed and McCorquodale (1992) observed seven distinct flow regimes during the filling of an empty channel (tailwater depth was increasing with time). Their set up was designed to study local scour phenomenon under conditions of zero

tailwater. Mohamed and McCorquodale (1992) observed rapid growth of mound with consequent rise in the effective tailwater level during regime 1 (jet attached to the bed) that resulted in the formation of a standing wave in the vicinity of the mound. At that time an explosive resuspension of bed material occurred and the flow changed to regime 2 (breaking wave and adverse hydraulic jump). Thereafter, for the next few minutes the flow regime changed sequentially through regime 2, regime 3 (unstable moving hydraulic jump on positive slopes with a plunging jet), regime 4 (wave jump and diving jet), and regime 5 (surface jet with entrainment from below) with almost equal duration for each regime. The plunging jet developed if the tailwater level was very low (Mohamed and McCorquodale, 1992).

Two other effects, namely, a backward moving dune formed due to the reversed current at the bed during regime 4 and increase in erosion of the mound. This reverse bottom current accelerated the growth and upstream movement of the dune (Mohamed and McCorquodale, 1992). According to Mohamed and McCorquodale (1992), the reduction of ambient water for entrainment caused the surface jet of regime 5 to re-attach to the bed resulting in regime 2. The regimes repeated themselves as long as the tailwater level was insufficient to produce hydraulic jump in the stilling basin and their duration changed with time. The jet behavior and duration of these regimes thus showed a strong dependence on the tailwater level (Mohamed and McCorquodale, 1992). Further, Mohamed and McCorquodale (1992) observed a lot of variability across the channel width along with a secondary current in the form of a large eddy with a vertical axis. It is interesting to note that their experiments were performed in two flumes having widths of 420 mm and 460 mm, which is very close to the width of the flume

used in the present study. This variability was caused by the bi-stable nature of the plane jet that resulted in non-uniform lateral distribution momentum inside the scour hole (Mohamed and McCorquodale, 1992).

A cursory evaluation of the test startup conditions in the studies noted above is quite varied. For example, Kells et al (2001) had the nozzle outlet plugged whereas, Mohamed and McCorquodale (1992) had the sluice gate closed until proper head and tailwater conditions were established. Following this, the nozzle was unplugged or the sluice gate opened to a predetermined extent to generate the jet flow. This requires a certain amount of time before a steady jet discharge can be established. Other researchers (e.g. Mazurek, 2001; Aderibigbe and Rajaratnam, 1998; Chatterjee et al, 1994; Rajaratnam, 1981) have first established the required tailwater conditions by filling the downstream side of the flume prior to generating the jet by a constant head arrangement or by applying a suitable head difference across the sluice gate opening. Johnston (1990) and Ali and Lim (1986) used a suitably sized aluminium sheet to cover the leveled bed in order to prevent it from being disrupted on commencement of the flow. The inflow was started, the flow and tailwater depths were then set to desired values following which the sheet was slowly removed. During the preliminary phase of this study, an effort was made to duplicate the test conditions adopted in previous studies such as the tailwater depth and jet exit velocity. However, the resulting scour pattern did not conform to earlier studies. Furthermore, there are several empirical scour prediction formulae that are available in literature for asymptotic conditions. These formulae provide for different predictions for identical flow conditions (see Appendix A) (Ahsan, 2003; Breusers and Raudkivi, 1991; Ali and Lim, 1986; Rajaratnam, 1981).

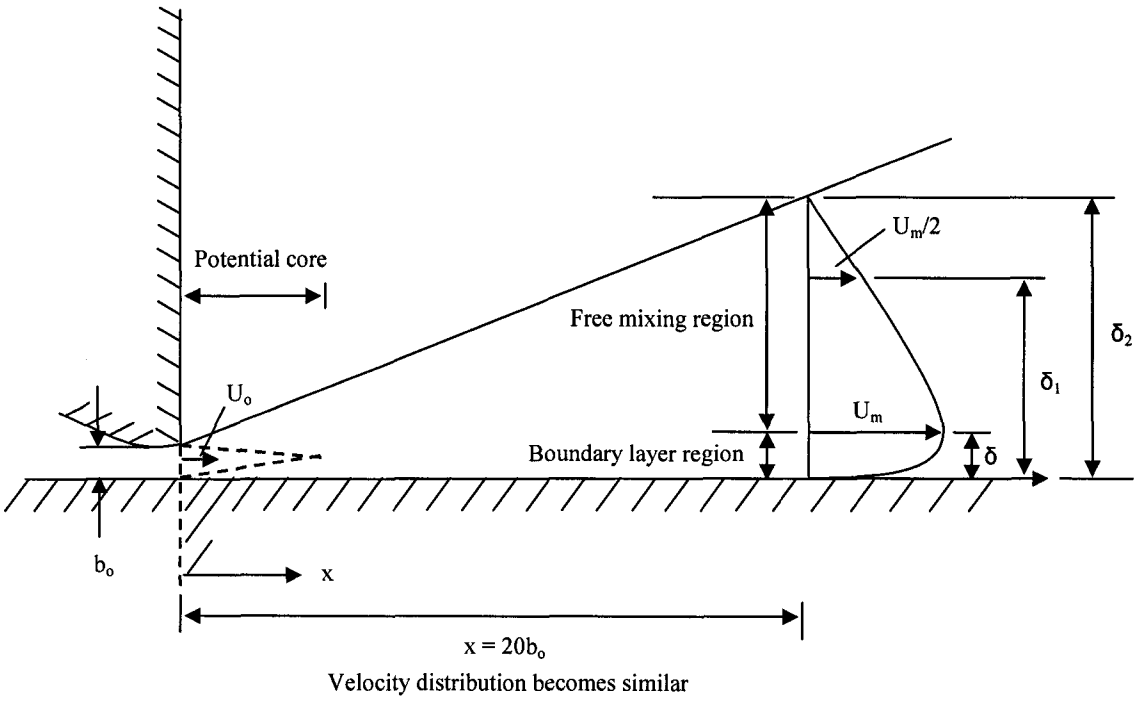

Figure 2-1: The plane turbulent wall jet (adapted from Rajaratnam, 1976)

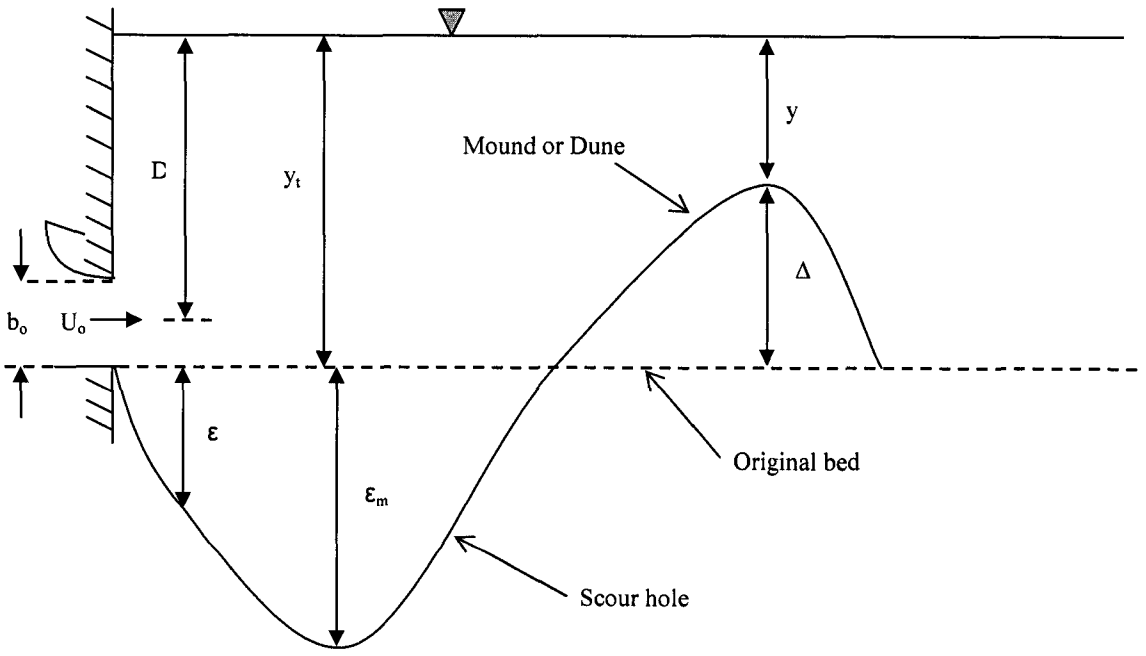

Figure 2-2: Definition sketch of scour hole profile

CHAPTER 3: EXPERIMENTAL SETUP AND EXPERIMENTS

3.1 Introduction

This chapter discusses the experimental setup, measurement procedures, and the testing program. All experiments were performed in the Hydraulics laboratory at the University of Windsor.

3.2 Experimental Setup

The experimental arrangement is shown in Figure 3-1. The experiments were carried out in a flume of rectangular cross-section of 0.4 m width, 0.9 m depth, and 15 m length (Figure 3-2(a)). A cohesionless sand bed, 0.4 m wide, 0.3 m deep and 2.4 m long, was set within the test section (Figure 3-2(b)). The sand bed had a Plexiglas wall on one side, which aided visual observations and optical access for the laser Doppler anemometer (LDA). The other parallel smooth wall was made of high density polyethylene. A rectangular nozzle of 0.4 m width was placed at the upstream end of the sand bed so that the bottom of the nozzle opening (25.4 mm) was level with the top of the sand bed. The nozzle is shown in Figure 3-2(c). Thus the jet created by flow through the nozzle was initially parallel to the bed. Water was supplied directly to a settling chamber by two 3-hp pumps from a 0.6 m wide, 1.25 m deep, and 1.7 m long recirculation tank. The recirculation tank is connected to the flume by a 0.15 m diameter, 2.95 m long pipe. The depth of water in the flume, or the tailwater depth, was controlled by a tilting gate, placed near the downstream end of the flume (2.35 m from the end of the sand bed).

The sand used for the experiments was approximately uniform in size with a median diameter D_{50} of 2.15 mm and had a geometric standard deviation σ_g of 1.28,

where $\sigma_g = \sqrt{D_{84} / D_{16}}$ and D_i is i^{th} percent finer. Figure 3-3 shows the grain size distribution for this sand. The sample indicated as "scour hole" in Figure 3-3, is one where the sand particles were scooped from the scour hole after a test run. It is seen from Figure 3-3 that no armoring is apparent, since the grain size curves are consistent between the samples.

Prior to the start of each test, the desired flow velocity was set by adjusting the valves on the downstream side of the pumps and the tailgate was set to the desired height. The velocity was then measured just outside the nozzle at the jet centerline and across the nozzle width at 40 mm intervals (to check for uniformity) using a 3 mm external diameter Prandtl tube connected to a U-tube manometer. The pumps were then shut off, the flume was drained, and the sand bed was leveled so that the top of the sand bed is even with the bottom of the nozzle opening. The sand bed was then prodded with a steel rod to ensure that there is no entrapped air and the bed was relevelled. Tap water was then used to refill the flume and re-circulation tank to the desired tailwater level. Flow was re-initiated by starting the pumps. Video images of the flow were acquired using a digital video camera.

3.3 Measurements

As mentioned earlier, the velocity measurements at the nozzle exit were carried out by using a 3 mm external diameter Prandtl tube connected to a U-tube manometer. The velocity measurements at different locations in the flow field were carried out with a single-component fiber-optic LDA (Dantec Inc) and the details are discussed in the following separate section. Measurements of the scour hole profile were taken at three sections across the width of the scour hole with time using a digital point gauge with a

resolution of 0.01 mm. The scour profiles were obtained at 3 h and 24 h for the lowest submergence. For higher submergences, the profiles were obtained at 36 h and at the asymptotic condition. All profiles were measured at three sections, i.e., along the jet centreline (denoted as CL), at a distance of 50 mm from the front Plexiglas wall (NW), and at 50 mm from the far wall (FW). To examine the flow patterns, water-soluble red dye was injected into the flow and the behavior was recorded using the video camera.

3.3.1 The laser Doppler anemometer

Laser Doppler anemometry is the measurement of fluid velocity by detecting the Doppler frequency shift of laser light that has been scattered by small particles moving with the fluid. A laser Doppler anemometer (LDA) system consists of a laser source, an optical arrangement, a photo detector that converts light into electrical signals and a signal processor. The LDA system was powered by a 300-mW argon-ion laser and was operated in backward scatter mode. The optical systems include a Bragg cell, a beam expansion unit and two lenses having focal lengths of 160 mm and 500 mm. The corresponding measuring volumes were $0.078 \times 0.078 \times 0.658$ mm^3 and $0.124 \times 0.123 \times 1.65$ mm^3 respectively. No artificial seeding was required due to sufficient particles present in the water. No measurements were possible at locations less than about $3b_o$ from the nozzle exit due to the restrictions imposed by the geometry of the transmitting optics and the flume support structures. Velocity measurements were taken from the commencement of the flow till the desired test velocity was reached for all startup conditions and then again at 6 h and 24 h. The velocity measurements were also taken at 24 h for the tests with high submergences and at 16 h for the test with the lowest submergence. Particularly, velocity profiles were obtained at a distance of $3b_o$ from the

nozzle opening, at the start of the mound and at the top of the mound for all the three sections, namely, CL, NW and FW. The uncertainties in the mean and turbulence intensity are estimated to be less than 1% and 2.5% respectively. The movement of fiber probe was facilitated by a manual traverse mounted on the flume support structure. The commercial LDA system has been used in several other studies and details are avoided for brevity (for example, see Tachie, 2001).

3.4 Testing Program

Experiments were carried out at various submergences (both high and low) in order to investigate the jet behavior and also evaluate the three-dimensional effects across the channel width. Furthermore, the effects of three different startup conditions were studied. This includes a gradual startup condition, a stepwise startup condition and an instantaneous startup condition. 'Startup' is defined as the commencement of flow through the nozzle on to the sand bed. A gradual startup condition is defined when the flow is commenced with the valves set for the minimum velocity at the nozzle exit, which are then gradually opened to reach the desired test velocity. The velocity is simultaneously monitored using the LDA. A stepwise startup condition is defined when the flow is commenced with the valves set for the minimum velocity at the nozzle exit. This velocity is maintained for a time period of 180 s, following which the valves are opened to increase the flow. This flow condition is once again maintained for 180 s following which there is another stepwise increase. This process is repeated till the desired test velocity is reached. An instantaneous startup condition is defined as a condition where the valves were set so that the desired test velocity is reached almost instantaneously once the flow is initiated.

Following a set of preliminary studies, it was noticed that for $8 \leq y_t/b_o \leq 20$, the visual flow pattern of the scour mechanism and its associated flow field along with the scour profiles were very similar to those seen by various researchers for deep submergences. However, for $y_t/b_o = 4$, the flow field and the scour mechanism was very similar to that of low submergences observed by Balachandar et al (2000). Consequently, it was decided to study the effect of startup conditions for $y_t/b_o = 4$ and $y_t/b_o = 20$ so that both types of flow fields are accounted for. A summary of the experiments performed is presented in Table 1. The flow Froude number (F_r) based on the jet thickness (defined as $U_o/\sqrt{gb_o}$) was 2.3, giving a densimetric Froude number (F_o) (defined as $U_o/\sqrt{gD_{50}(S-1)}$, where S is the specific gravity of the sediment) of 6.2 and a jet Reynolds number ($\mathrm{Re}_j = U_o b_o/\nu$) of 32500.

Table 1: Details of experiments

Test	Startup condition	U_o (m/s)	y_t (mm)	y_t/b_o	t_d (h)	Notes
A	Gradual	1.16	101	4	24	a
B	Stepwise	1.16	101	4	24	a
C	Instantaneous	1.16	101	4	24	a
D	Instantaneous	1.16	203	8	72	*
E	Instantaneous	1.16	305	12	48	*
F	Gradual	1.16	508	20	48	*
G	Stepwise	1.16	508	20	48	*
H	Instantaneous	1.16	508	20	48	*

'*' signifies one complete test run till asymptotic state of scour is reached
'a' signifies that the test was terminated prior to asymptotic state since the mound reached the end of the sand bed

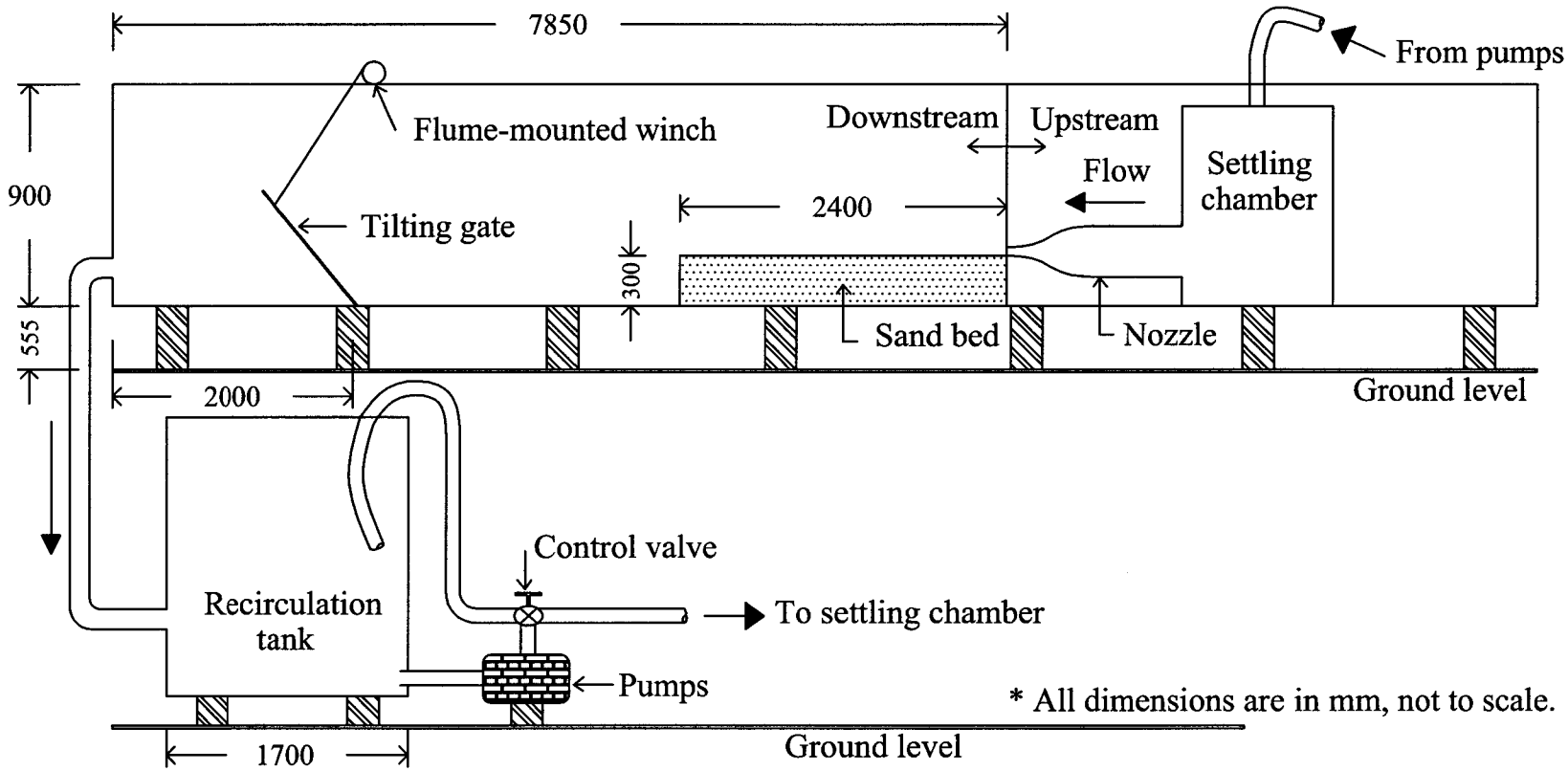

Figure 3-1: Experimental setup

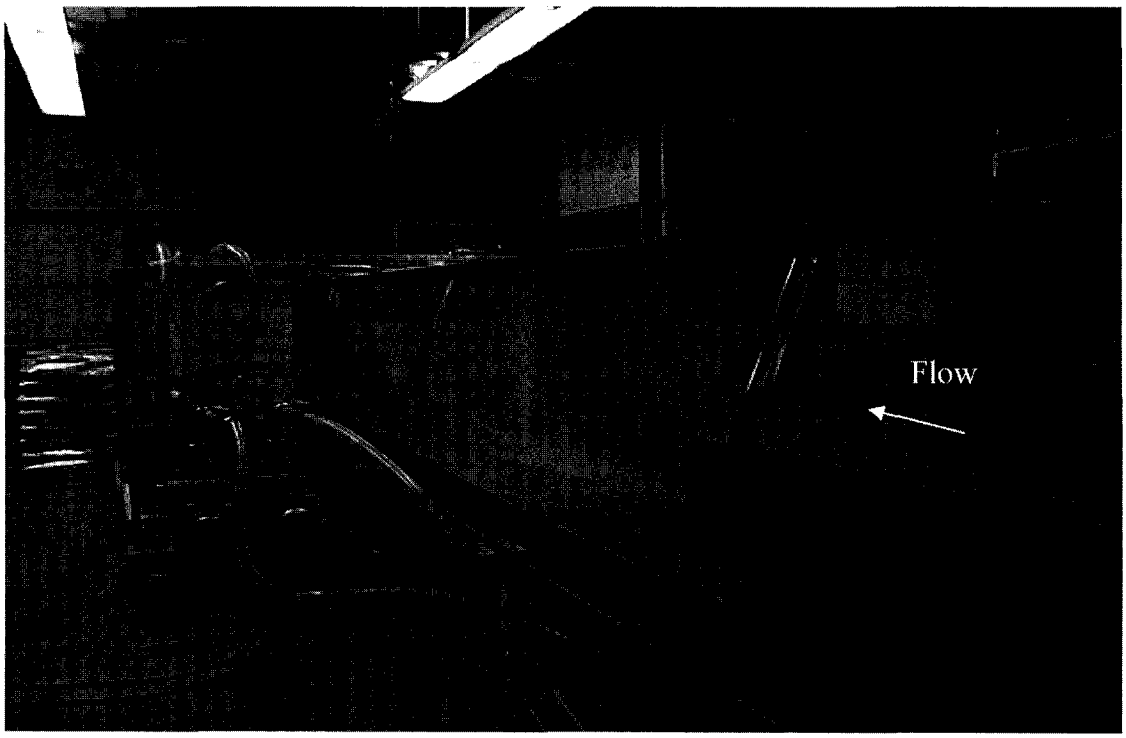

(a)

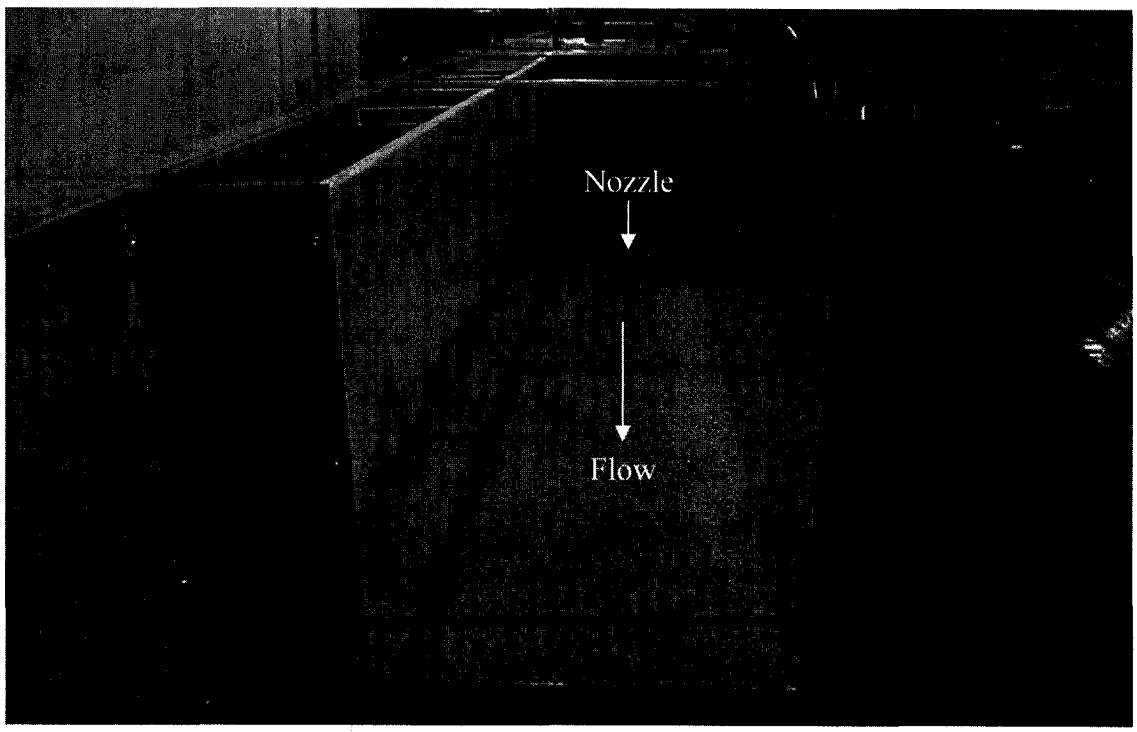

(b)

Figure 3-2: Experimental setup (a) flume and pump arrangement (b) sand bed (c) nozzle

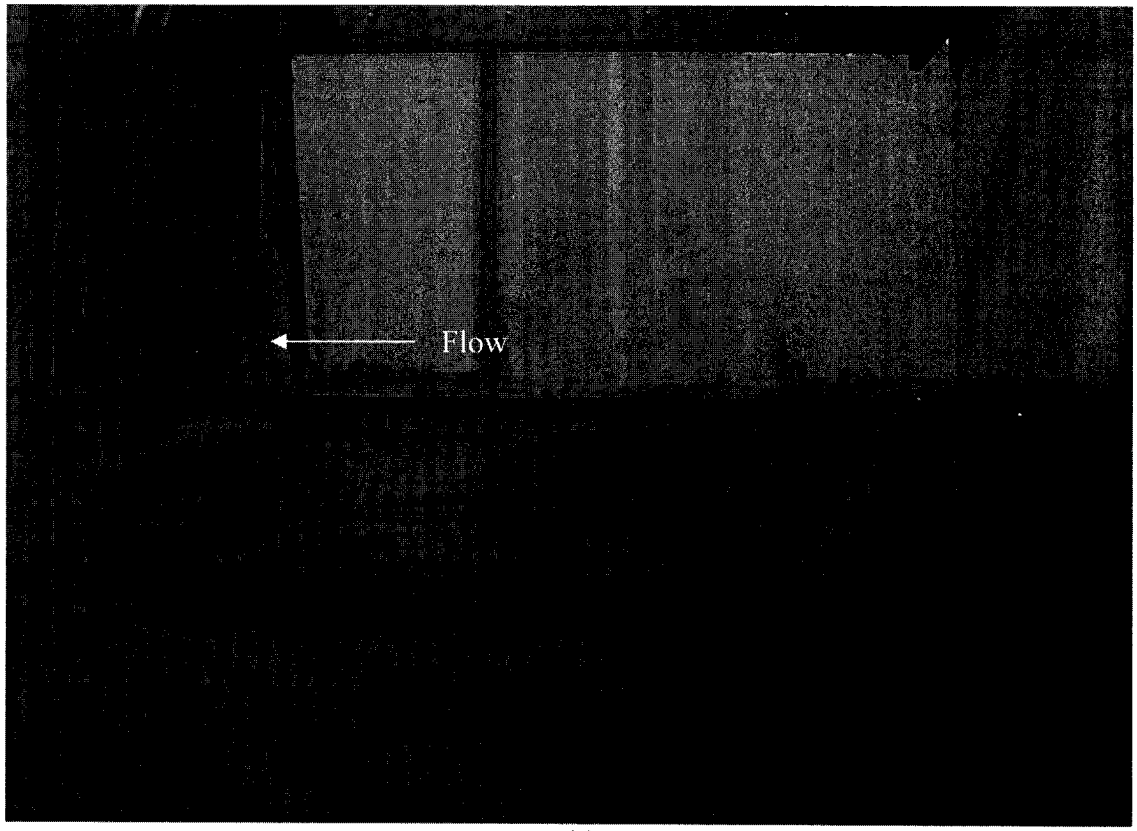

(c)

Figure 3-2: cont'd

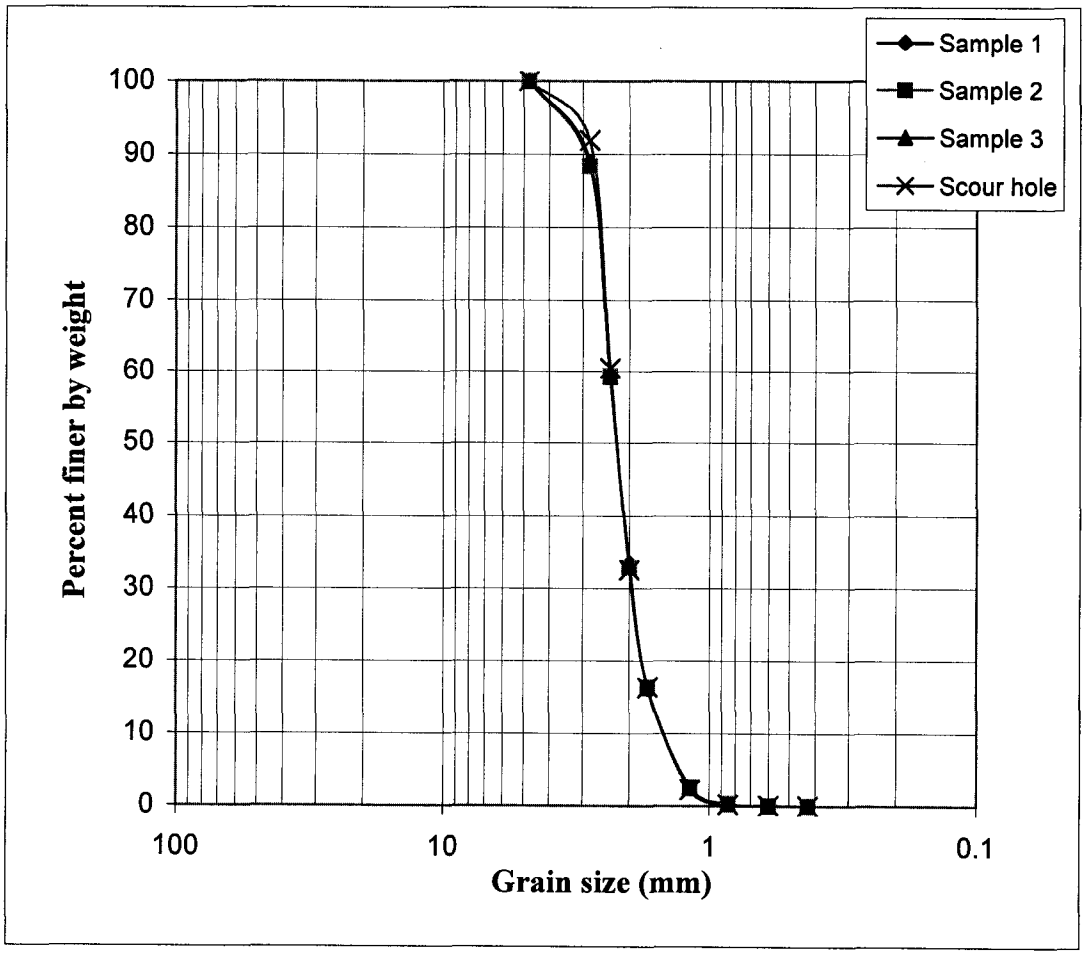

Figure 3-3: Grain size curves for the sand used in experiments

CHAPTER 4: RESULTS, ANALYSIS, AND DISCUSSION

4.1 Introduction

The experimental observations and results are presented in this chapter. Detailed observations of the scour hole development and the associated regimes of flow for a varied range of submergence (both high and low) are presented. The effects of test startup conditions are discussed along with the analysis of velocity measurements made by the laser Doppler anemometer. Finally, observations and analysis of the effects of submergence is presented.

4.2 Visual observations of the flow field

4.2.1 High submergence

The flow field for $y_t/b_o = 20$ was found to behave as deeply submerged (i.e. no flicking towards the free surface) and the scour profile development was stable to the end of the test. The forthcoming discussion is based on the observations of the instantaneous startup conditions. Any variations from these observations for other startup conditions are noted at the appropriate sections in the text. The jet as it exists from the nozzle was initially parallel to the bed and scour commences. Dye visualization indicates that the jet follows the bed contour and appears attached to the bed as seen in Figure 4-1a. After a short duration, the dye streakline pattern takes the shape that is normally encountered in separated flows such as that noticed in flow past a backward facing step (Eaton and Johnston, 1981), as seen in Figure 4-1b. For backward facing steps, the reattachment point fluctuates back and forth with a mean location being around six times the step height. In this study, this fluctuation is enhanced possibly due to the fluidization of the

bed in the reattachment region due to flow impingement. One can say that the position of the reattachment point is unsteady and the large scale changes in the reattachment length give the resemblance of the jet impingement point moving longitudinally back and forth. At no instant the jet flicks between the free surface and the sand bed, as was noted in earlier low submergence studies (such as Balachandar et al., 2000). As the reattachment point nears the nozzle, the flow resembles a bed jet that conforms to the shape of the scour profile. Figure 4-2 shows a series of events starting with an attached bed jet (Figure 4-2a). As the impingement point moves forward, scouring action is distinctly visible (Figure 4-2b) and the jet gradually tends to become horizontal (Figure 4-2c). The impingement now occurs directly on the mound resulting in its partial breakup. A strong clockwise eddy as viewed from the near wall was observed above the impingement point. The sediments that would rise in suspension due to the impinging action follow the eddy, particularly depositing on the mound and, some particles roll over the downstream face of the mound. When the jet is nearly horizontal, a significant portion of the sediments fall back into the scour hole due to the partial breakup of the mound. Simultaneously, no movement of the bed material was observed from the jet exit to a distance up to the location of the maximum scour hole depth. Following the partial breakup of the mound, the reattachment point then begins its movement towards the nozzle (Figure 4-2e, f) and eventually the flow once again resembles that of an attached bed jet. Figure 4-3 shows the changes in scour profile shape with the change in the impingement point. A smooth scour profile (Figure 4-3(a)) can be seen for a bed jet when the jet follows the bed contour, whereas when the jet impingement point moves forward, a distinct kink in the scour profile is noted (Figure 4-3(b)).

4.2.2 Low submergence

In case of the lowest submergence ($y_t/b_o = 4$), as mentioned earlier, the flow field and the scour mechanism were very similar to that observed by Kells et al (2001). The scouring process consists of two distinct phases, namely, the digging phase when the jet is near the bed (Figures 4-4a, b, c) and a refilling phase, when the jet flicks to the free surface (Figure 4-4d, e, f). To enhance visualization, the dye flow patterns are indicated by arrows to show the mean flow. During the digging phase, the jet behaves like an attached bed jet and there is scouring of the bed leading to the formation of a scour hole and a flattened mound. It should be mentioned that the impingement point does travel back and forth longitudinally. After some time, the jet suddenly flips towards the free surface to become a surface jet (see Figure 4-4d) causing a wavy action at the water surface. Refilling of the scour hole is observed during the surface jet regime as also noted by previous researchers.

Comparison of the flow fields at low and high submergences (Figures 4-2 and 4-4) indicates that the flow patterns are different and each on its own is quite complex. It is noteworthy that for higher submergences a distinct mound region is a dominant feature, whereas, for lower submergences the mound is essentially long and flattened out. It should be remarked that no large wave action at the free surface was noted in flows with deep submergences. More details are provided in a later section.

4.3 Effects of test startup conditions

As indicated earlier, three startup conditions, namely, gradual, stepwise and instantaneous, were adopted for the tests with $y_t/b_o = 4$ and $y_t/b_o = 20$. Some visual observations with respect to test startup conditions showed that the initial rate of scouring

was lower for gradual and stepwise startup conditions as compared with the instantaneous condition. This is to be expected as the test is directly commenced at a higher jet exit velocity for the instantaneous condition. Figure 4-5 shows the velocity time history for the three startup conditions at the highest tailwater depth. The measurements were conducted at $x/b_o = 3$ along the nozzle centreline. Figure 4-5a shows that for the instantaneous startup condition the velocity is highly turbulent ($u_{rms}/U_o \approx 22\%$) showing large scale changes about the mean. The white solid line represents the mean velocity. The desired flow velocity is attained in a very short time span and the mean does not change significantly after that. Figure 4-5b shows the velocity time history for the stepwise startup condition. The increase in velocity by the stepwise adjustment of the valve is clearly seen. At the first setting of the valve there was no significant scour. At the second step, as scour commences, there is a slight increase in the mean velocity accompanied by an increase in the velocity fluctuations. With further opening of the valve, the mean velocity is gradually increased and at the final step velocity distribution is similar to that noticed in the instantaneous condition. Figure 4-5c shows the time history for gradual change in startup condition. The velocity data for the first 600 s are re-plotted in Figure 4-6 for the gradual startup condition. To enhance visualization, a line based on adjacent averaging is drawn through the data. The data clearly indicates that up to about 150 s when there is no large scale scour, there is a gradual increase in velocity with increased opening of the valve. However, beyond 150 s one notes a significant dip in the mean velocity accompanied by large scale increase in turbulence. Following this, any increase in opening of the valve causes a further increase in the velocity. The increasing discharge provides for velocities to be greater than the critical velocity needed

for large scale scour and correspondingly the fluctuations about the mean increase significantly. For t > 400 s, one can note the presence of low frequency fluctuations (imposed on the high frequency turbulence), the origins of which are discussed in the following paragraph. It should be noted that the desired velocity was attained after t = 2000 s in the case of stepwise startup condition (Figure 4-5b) and after t = 600 s for gradual startup condition (Figure 4-5c).

In order to better understand the influence of the startup condition soon after the desired velocity is attained, the velocity time history is analyzed at time t = 40 minutes at the nozzle centreline and at a distance of $3b_0$ from the nozzle exit. At this time, the flow has attained the desired velocity and no more changes are being made to the operating conditions. To distinguish turbulent features of the jet from the movement of the reattachment point, a low pass Fast Fourier Transform filtering of the data was carried out and the filtered information is presented as a solid white line in Figure 4-7. In these graphs, the occurrence of higher velocities indicates the tendency of the jet to be parallel to the initial bed at the point of measurement. The occurrence of larger turbulence indicates that the jet is bent towards the bed and the measurement point is possibly in the entraining zone of the jet. Comparing Figures 4-7a and 4-7b with Figure 4-7c, one can note the occurrence of a larger number of peaks (in the filtered data) in the same time interval for gradual startup condition. This indicates that though the mean flow is similar there are still features in the flow field that have not subsided to the conditions noted in the instantaneous flow. A similar analysis was carried out at other time intervals for the instantaneous condition (Figure 4-8), and one can note that the flow features gradually change with no significant difference in the filtered data beyond time t = 6 hours. Further,

a similar behavior was noticed for the other two startup conditions and is not shown here for brevity.

To further understand the flow features that are created by the movement of the reattachment point, the velocity histogram at the nozzle centre and at ± 15 mm from the nozzle centreline are presented for $y_t/b_o = 20$ in Figure 4-9. It is clear that a significant number of velocity realizations are obtained around 0.2 m/s at 15 mm above the nozzle centreline while a large number of velocity realizations are obtained at 1 m/s at the nozzle centreline. A near bi-modal velocity distribution can be seen at 15 mm below the nozzle centreline. It is important to recognize that there are a significant number of negative velocity realizations below the nozzle centreline. Collectively, the three graphs indicate that as the impingement point moves back and forth there are small changes in velocity measurements at the centreline of nozzle while above and below the nozzle show changes that conform to the movement of the jet. Figure 4-10 shows the velocity histogram obtained in the flow field close to the bottom of the scour hole near the location of the maximum scour depth. The bi-modal peak once again represents negative and positive velocities, indicating the movement of the reattachment point in both directions and is similar to that obtained below the nozzle.

The velocity features (time history) near the nozzle exit for all startup conditions at the lowest submergence (Figure 4-11) are very similar to that noticed at the highest submergence. The features noticed in the gradual startup condition in Figure 4-6 also occur at lower submergence. However, to clarify the digging and refilling phases (i.e., flipping of the jet between the sand bed and the free surface) velocity measurements were conducted at a station of $3b_o$ from the nozzle. To this end three points were chosen, one

along the nozzle centreline and the other two at ± 15 mm from the nozzle centreline. Figure 4-12a shows the velocity time history at 15 mm above the nozzle centreline. The first 100 s reflect the measurements in the refilling phase and the jet is directed upwards. As the jet flips towards the sand bed and digging commences, the velocity measurements are different from that noticed for $t < 100$ s. Further, the duration of digging is short and once again refilling commences after $t = 150$ s. Figure 4-12b shows the measurements along the nozzle centreline where it is difficult to distinctly interpret the digging and refilling phases. Figure 4-12c shows velocity measurements below nozzle centreline and one can note higher velocities during the digging phase. It is also noteworthy that on comparing the data above and below the nozzle, during the refilling phase there is a large spread ($0 \leq V$ (m/s) ≤ 1.4) in the instantaneous velocity measurements in Figure 4-12a. The velocity time history during the digging phase of Figure 4-12c ($125 < t$ (s) < 200) is replotted in Figure 4-12d, which indicates that there are low frequency fluctuations in the jet similar to that noticed in Figure 4-7c, though the frequency of fluctuations is higher.

Figure 4-13a shows the effect of the startup conditions on scour at the lowest submergence at three hours from the commencement of the flow. Due to the prevailing short time scale feature of the digging phase and the occurrence of refilling over a longer period of time, the scour profiles corresponding to the refilling phase are used as a basis of discussion. One can notice the occurrence of an intermediate mound very close to the nozzle exit, which is gradually flattened out due to the refilling action. There are no large scale differences in the profiles measured that can be attributed to startup conditions. However the stepwise and gradual startup conditions indicate that the mound was slightly higher and longer. It was noticed during the test that the digging phase continued for a

longer time for these two startup conditions while for the instantaneous condition the first refilling phase commenced quite quickly. Consequently, there has been more digging action and this is reflected in the profiles. This is an important aspect to note while comparing scour profiles from different studies carried out with different startup conditions. Figure 4-13b shows the profiles along the nozzle centreline for the three startup conditions at 24 hours from the commencement of the test for lowest submergence. No significant differences can be found in the profiles and any minor differences that were noticed earlier have vanished. Figure 4-13c shows the scour profiles at the three startup conditions at 36 hours for the deepest submergence. Clearly the effects of test startup conditions are not manifest at t = 36 h. One can conclude that the effects of test startup conditions do not influence the long term scouring process.

Figure 4-14a shows the velocity profiles obtained along the nozzle axis at the mouth of the nozzle ($x = 3b_o$) for all the three startup conditions after the desired test velocity has been attained. The figure clearly shows that the prevailing test conditions are nearly identical for all startup conditions. Similarly Figures 4-14b and 4-14c respectively show velocity profiles at the start of the mound ($x/b_o \cong 20$) and at the top of the mound at 24 hours from the commencement of the test. Collectively Figure 4-14 indicates that the flow evolves to a similar state independent of the startup conditions and conforms to the conclusion drawn from the scour profiles.

4.4 Effects of submergence

Figure 4-15a shows the scour profiles along the centreline of the nozzle for the three higher submergences that show overall similarity in flow behavior. At the two larger tailwater ratios ($y_t/b_o = 12$ and $y_t/b_o = 20$) the profiles are more or less similar in

the scour hole region while they are slightly different in the mound region. Figure 4-15a also shows that the scoured region at $y_t/b_o = 8$ is much larger for the same time period. For the range of higher tailwater conditions tested in the present study ($y_t/b_o \geq 8$) one can note that there is more scour at lower submergences. It would appear that the volume of material scoured out of the hole is not equal to that in the mound, especially at the higher submergences. This is a consequence of the mound region showing variability across the cross section of the flow. This aspect is discussed later. To this end, Figures 4-15b to 4-15d show the profiles at the three higher tailwater depths including their variation across the flume cross-section. As indicated earlier, CL denotes the nozzle centreline, NW is close to the near wall and FW is near to the farther wall. It is clear from these three figures that beyond the scour hole region the profiles are different across the cross-section. There is a depression in the mound region which occurs slightly upstream of the mound peak and extends downstream. Hence, the centreline profile shows a smaller mound than noticed at NW and FW. The depression in the mound region is reduced as the tailwater depth decreases. Since the scour profiles at the lowest tailwater depth are different they are presented in a separate figure (Figure 4-16). The profile is shown for time t = 24 hours as the end of the mound is very close to the end of the sand bed. It is clear from this figure that there is no variability in the mound region across the flume section.

In an effort to further analyze some of the variability noted in the scour profiles, additional velocity measurements were conducted. To this end, once again three stations, namely, at a distance of $3b_o$ from the nozzle, at the start of the mound and at the top of the mound were chosen. At each station, profiles were obtained at CL, NW and FW. The

measurements at $x = 3b_o$ for various tailwater conditions is shown in Figure 4-17 for t = 24 hours. No distinct non-uniformity in the velocity distribution is noticed at $x = 3b_o$. It should be remarked that Mohamed and McCorquodale (1992) have suspected that the non-uniformity in scour noted in their study was due to lateral variation in jet momentum. This lateral variation of momentum was not noticed at $x = 3b_o$. At each submergence, though the valve opening (fully open) is set to yield the same discharge at the nozzle exit, the peak value increases with decreasing submergence. Further, the location of peak value also changes from below the nozzle centreline to above the nozzle centreline at the lowest submergence. However, there is no distinct variability across the flow cross-section at any given submergence. The larger peak noted at $y_t/b_o = 8$ provides for larger scour potential downstream. Figure 4-18 shows the corresponding velocity profiles at the start of the mound. At any given submergence, there is a clear difference in the profiles between the nozzle centreline and that observed at the walls. This will cause a lateral variation in momentum distribution. However, this variation is symmetrical about the jet axis. The difference in the velocity profiles seems to increase with decreasing submergence. The measurements at $y_t/b_o = 4$ is not shown here as the flow field is different from the other three tailwater ratios. Visual observations indicate that in the region from the maximum scour depth to the start of the mound there is a presence of more intense impingement (hence scouring) on either sides of the centreline though the scour profile is nominally two-dimensional and uniform across the flow cross-section. The higher velocities noticed at NW and FW in Figure 4-18 confirm that there should be more scouring action in the region close to the walls. However, due to the rapid movement of the impingement point and sand particles tending to fall back into the scour

hole, the profiles shown in Figure 4-15 do not reflect major changes between the walls and the centreline in the region $200 < x\ (mm) < 600$.

Visualization of the mound region indicates that there are two peaks with a distinct trough at the centreline for high submergences (see Figure 4-19). The peaks are located at the walls. With decreasing submergence, the trough region appears to be more filled and the difference in height between the trough and the peaks is reduced and the mound tends to flatten out. Further, the slope of the upstream face of the mound increases with decreasing tailwater ratio. This is particularly prominent in the slopes of the mound noted near the walls for $y_t/b_o = 12$ and $y_t/b_o = 20$. Figure 4-18b shows the velocity measurements at $y_t/b_o = 12$. As the flow climbs up the mound and noting that the slope of the mound in the central region is around 17.6^o while that closer to the walls is 22.5^o, the flow is likely to undergo a greater acceleration (due to decrease in overall area) near the wall regions. This is reflected in the higher velocities at the NW and FW. Figure 4-20 shows the mean velocity profiles at the top of the mound and is consistent with the fact that all three profiles at a station get closer together as the tailwater decreases. Observations by dye injection indicate the movement of the dye from the centreline towards the flume walls in the mound region. Moreover, the negative values of mean velocities at jet centreline (Figure 4-20a) indicate that the flow is upstream in the trough region.

Figure 4-21 shows a collection of histograms at the station $x = 3b_o$. Data are shown at the nozzle centreline and at two locations above and below the nozzle centreline. On comparing these histograms it is quite clear that the jet behavior is more or less similar along the jet centreline (middle column in Figure 4-21). However, the flow

characteristics depend on the level of submergence. Besides the obvious flicking of the jet noticed at the lowest submergence, there are changes between the other three tailwater ratios, which can be considered as nominally deep. For example, below the nozzle centreline one can note reductions in negative velocities with decrease in submergence. It should also be remarked that the velocity histogram in Figure 4-21d are obtained in the refilling phase. Finally, Figure 4-22 shows low pass filtering done on the velocity time history near the start of the test for different submergences. It can be clearly seen that the number of peaks noticed in the low pass filtered data increase with decreasing submergence which shows that the movement of the impingement point is more rapid with decreasing submergence.

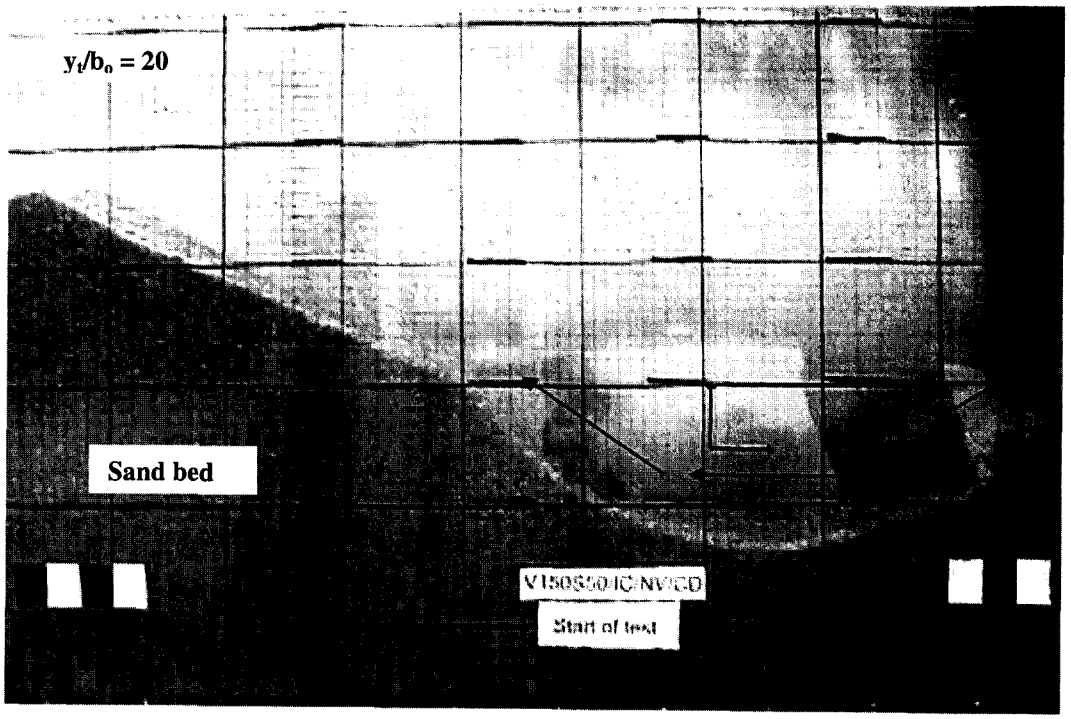

Figure 4-1 (a): An attached bed jet.

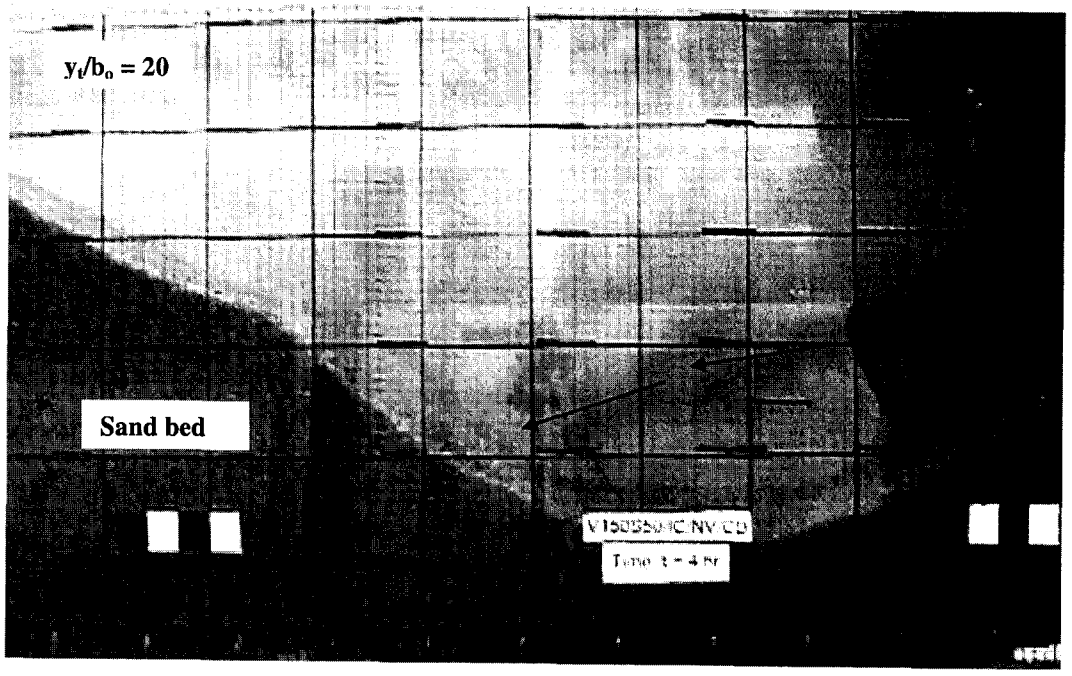

Figure 4-1 (b): An impinging jet.

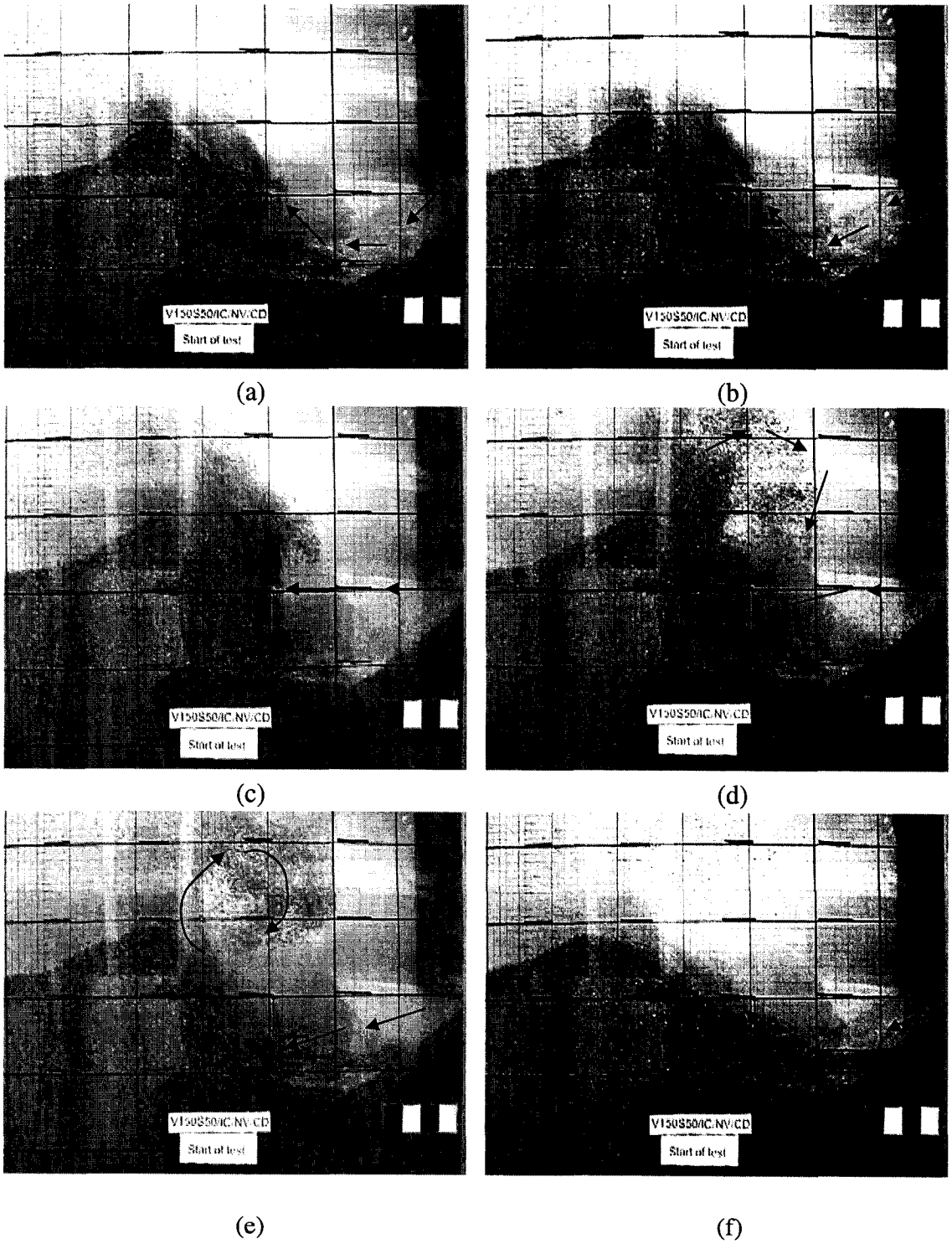

Figure 4-2: Series of events to show movement of the impingement point for $y_t/b_o = 20$ (a) at 17 sec. (b) at 18 sec. (c) at 19 sec. (d) at 20 sec. (e) at 21 sec. (f) at 24 sec.

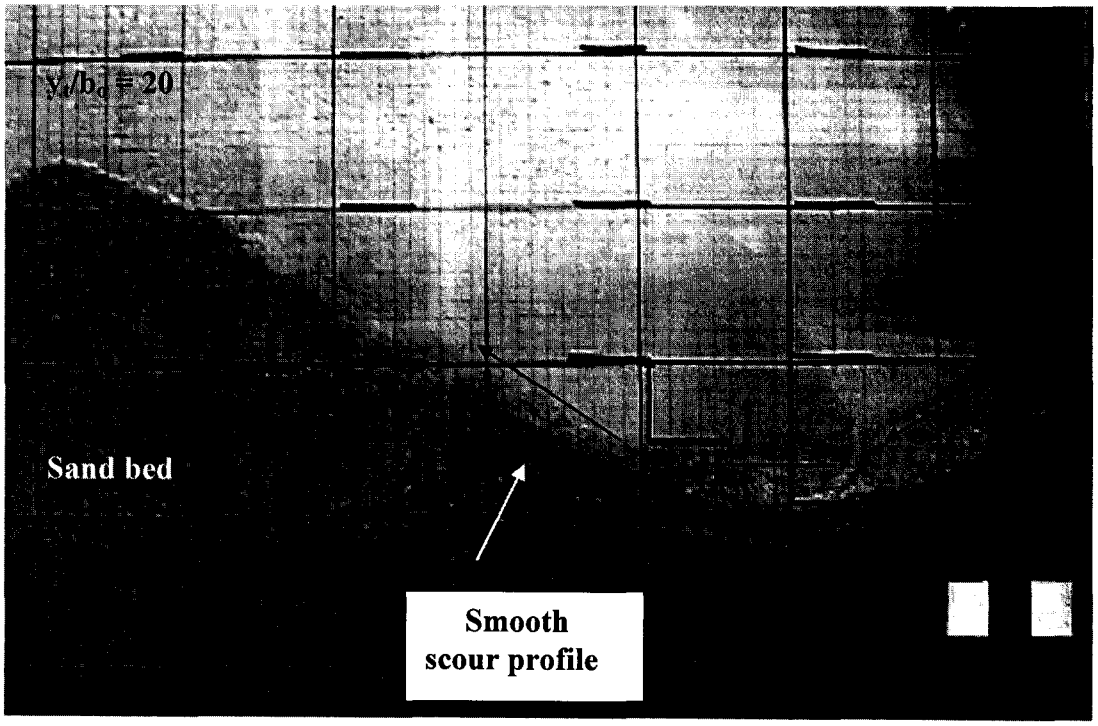

Figure 4-3 (a): Smooth scour profile

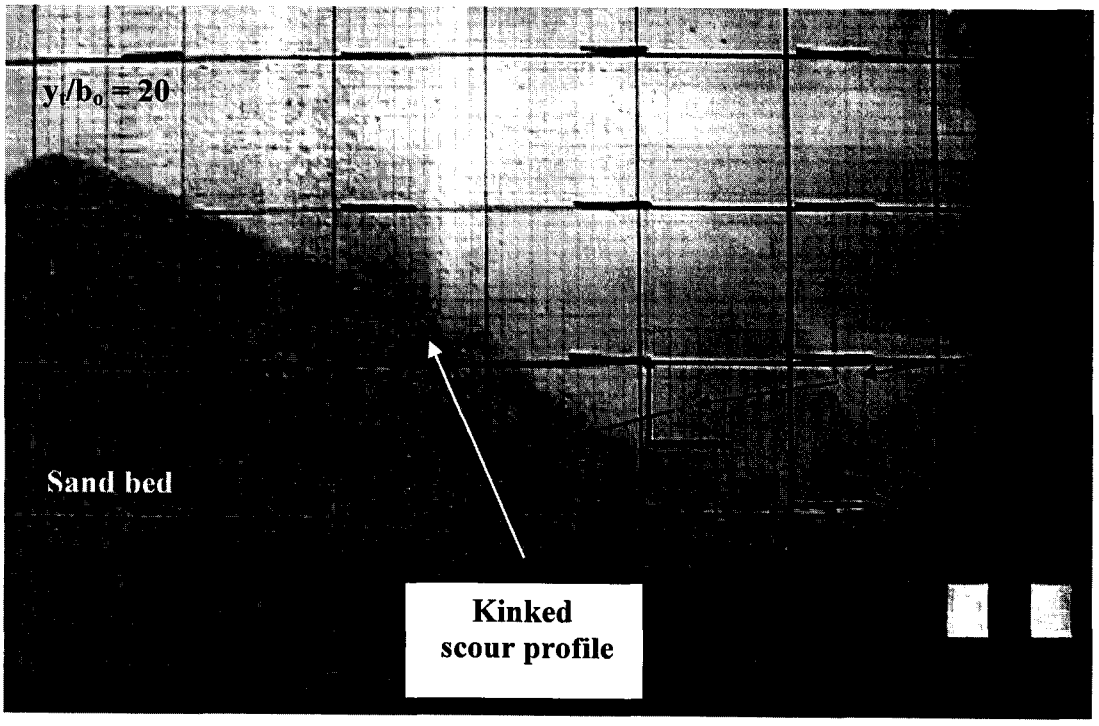

Figure 4-3 (b): Kinked scour profile

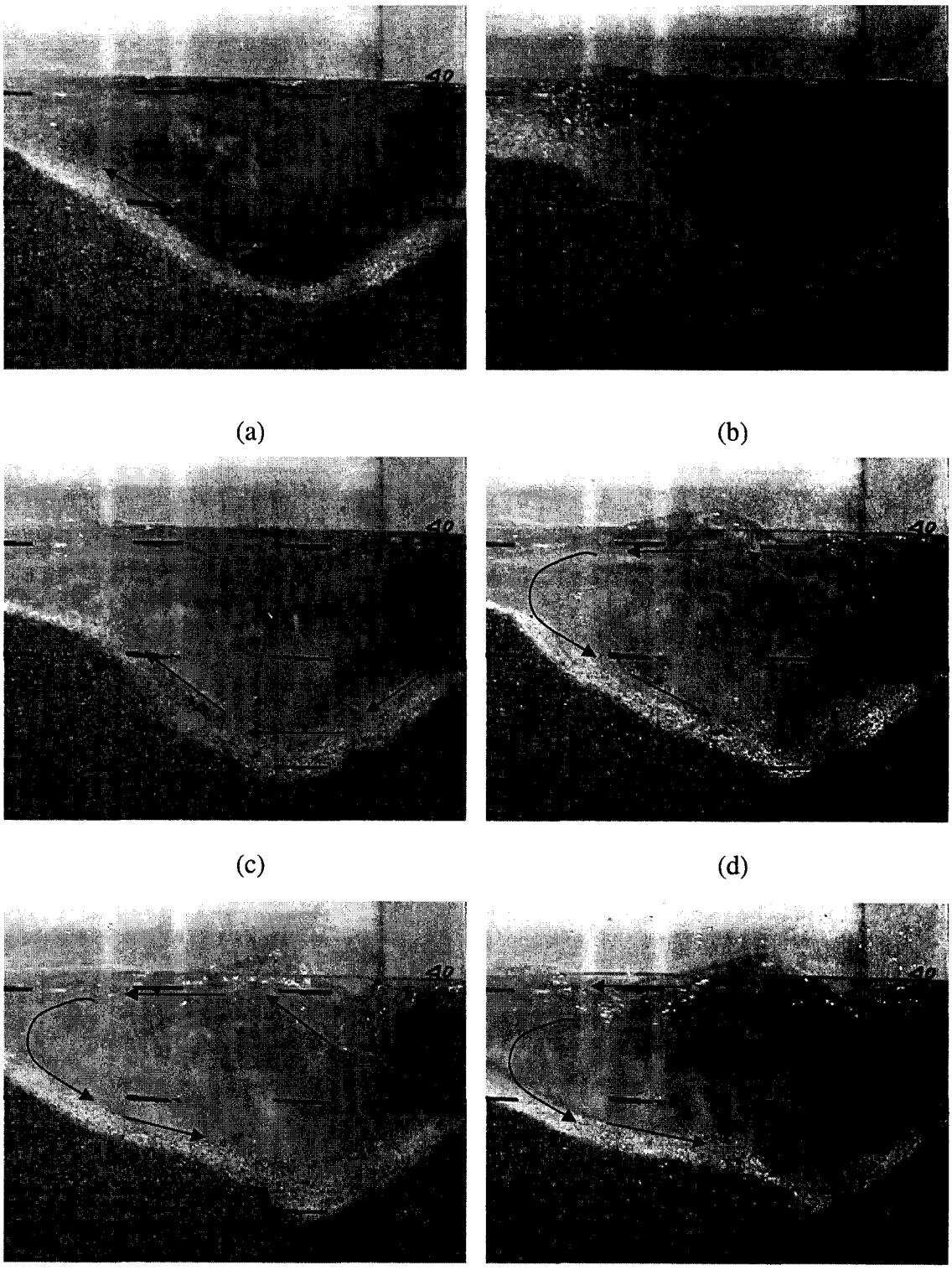

Figure 4-4: Transition from digging phase to refilling phase for $y_t/b_o = 4$ (a) at 185 sec. (b) at 198 sec. (c) at 213 sec. (d) at 215 sec. (e) at 225 sec. (f) at 305 sec.

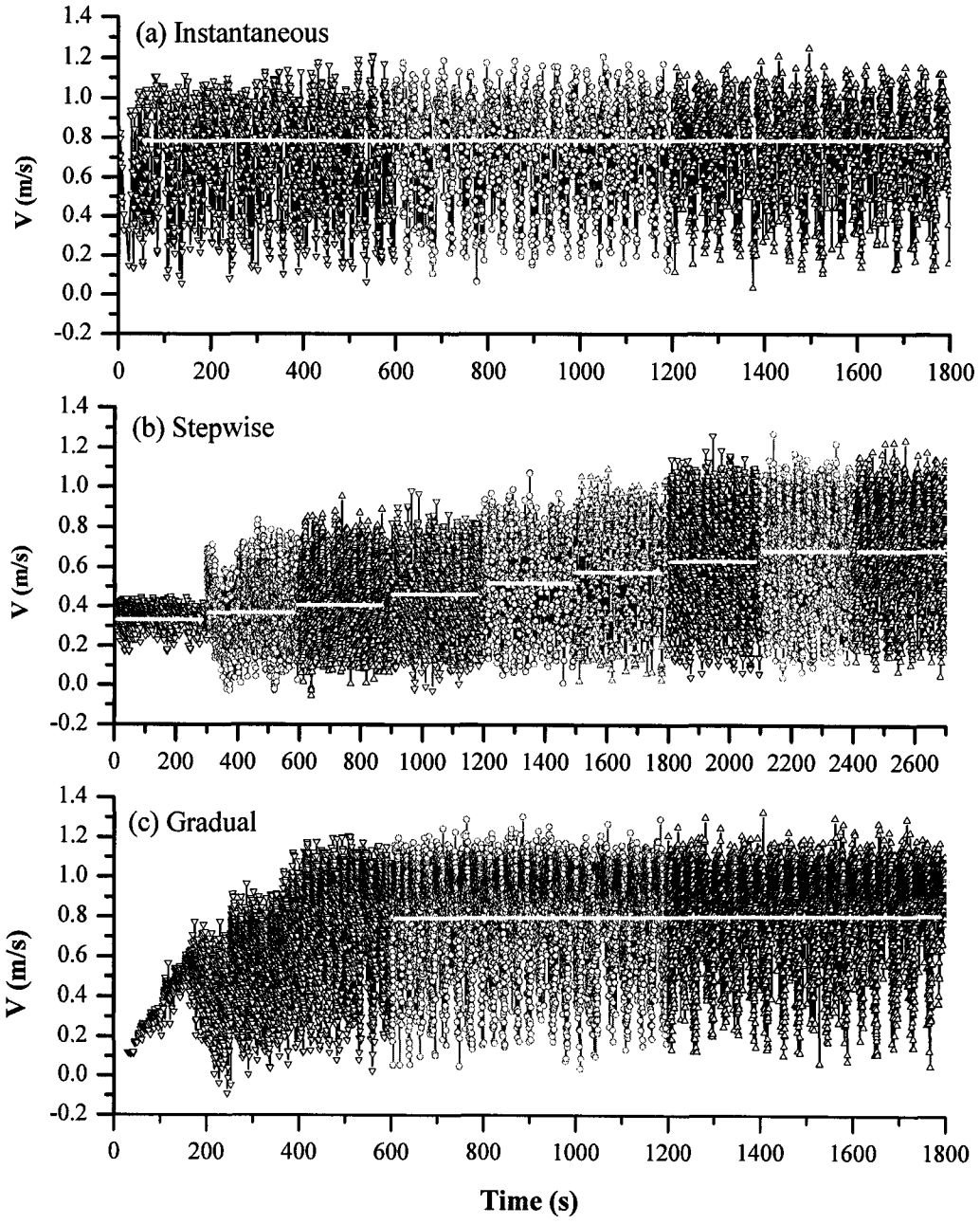

Figure 4-5: Effect of test startup conditions for $y_t/b_o = 20$

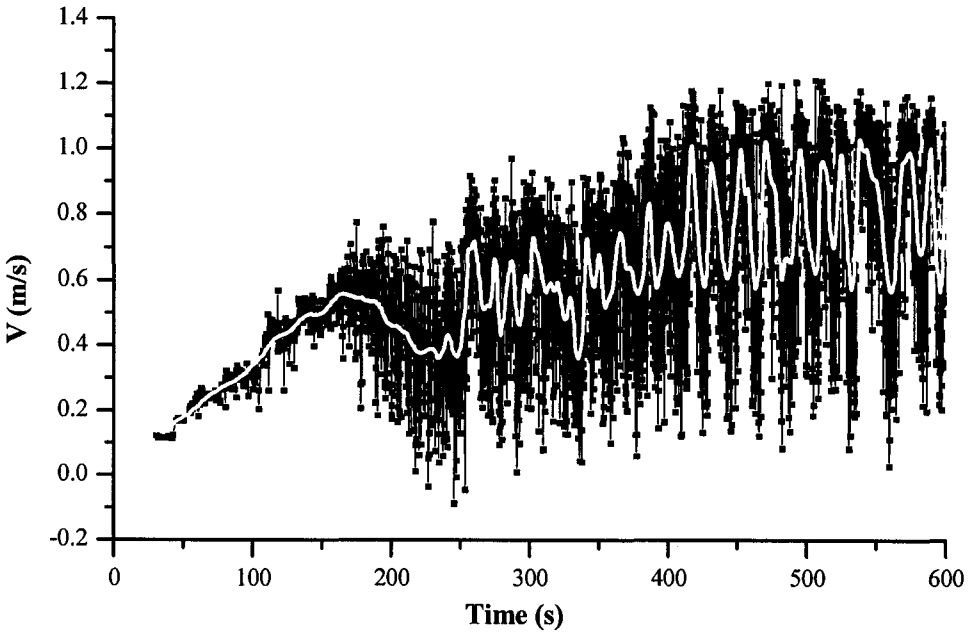

Figure 4-6: Gradual startup condition up to t = 600 s for $y_t/b_o = 20$

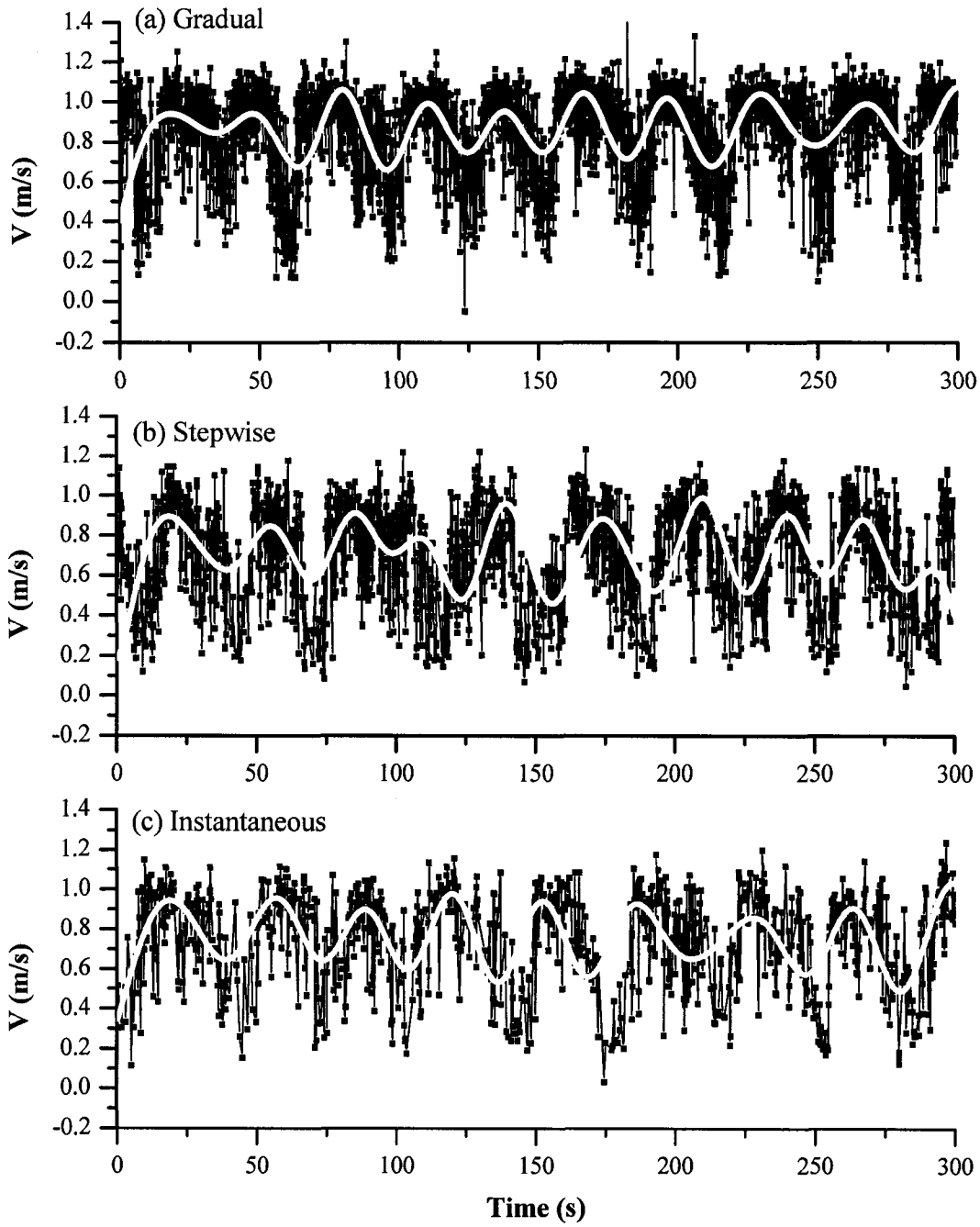

Figure 4-7: Comparison of different startup conditions for $y_t/b_o = 20$ at t = 40 min

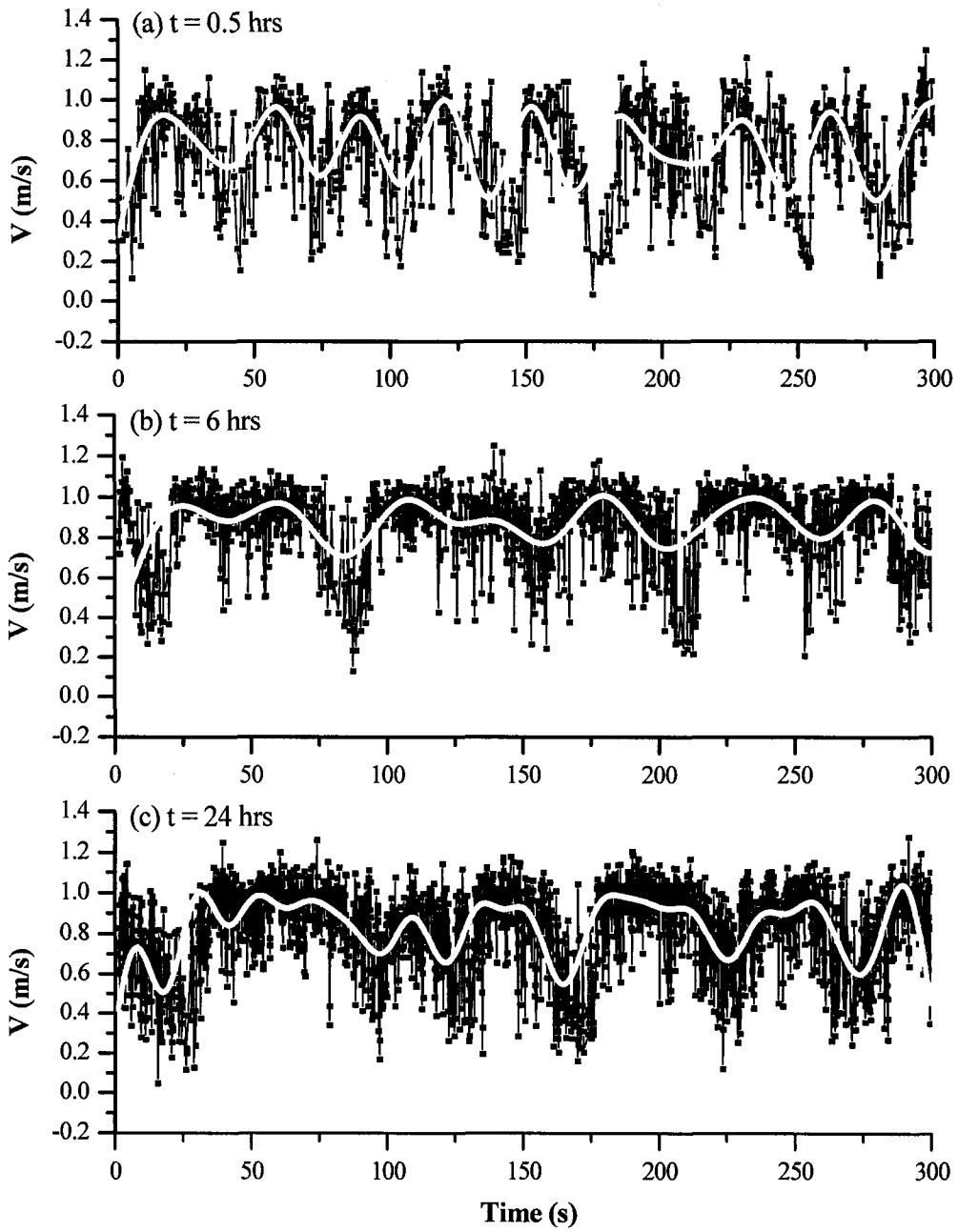

Figure 4-8: Velocity time history for instantaneous startup condition at $y_t/b_o = 20$

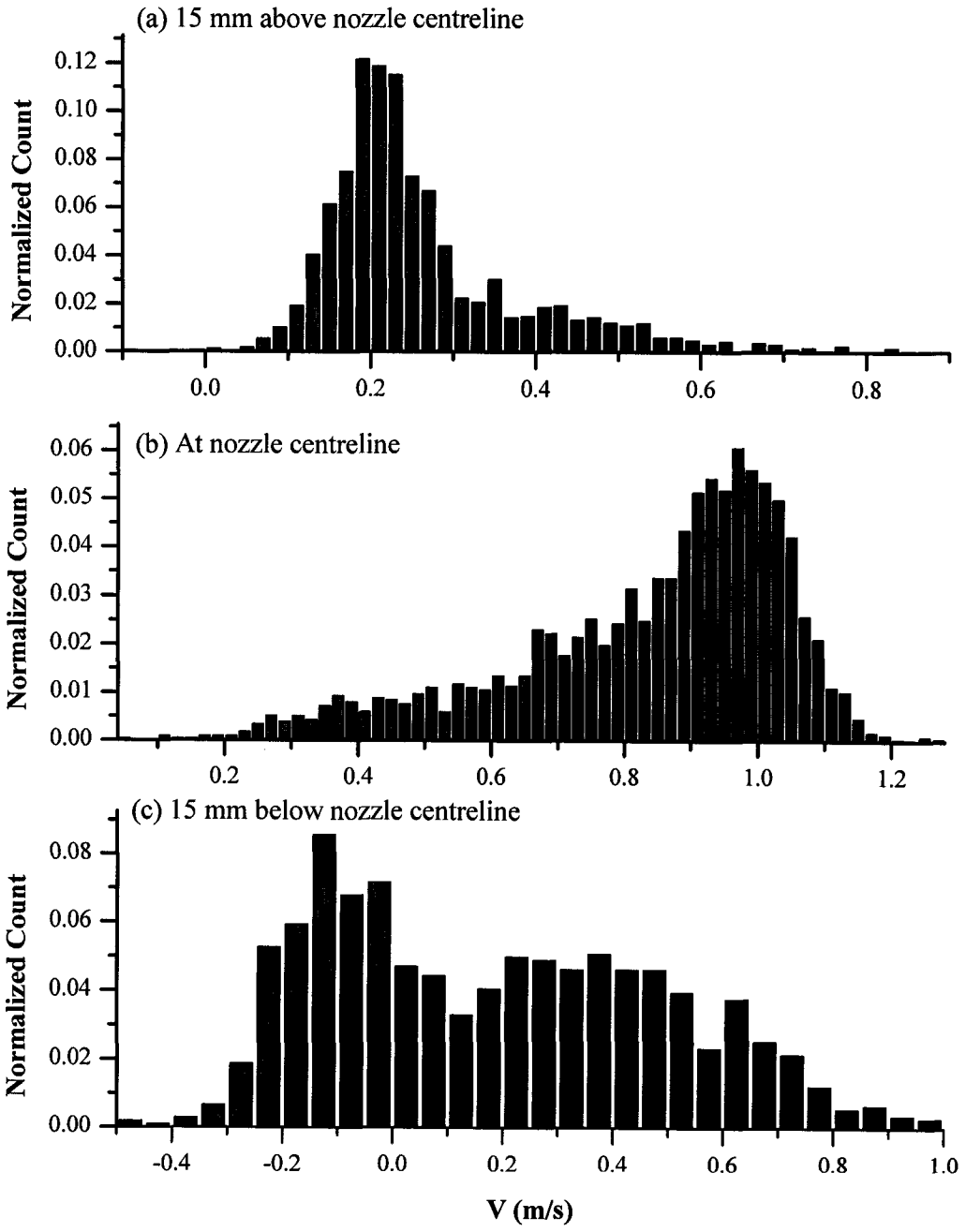

Figure 4-9: Velocity histograms for instantaneous startup condition at $y_t/b_o = 20$

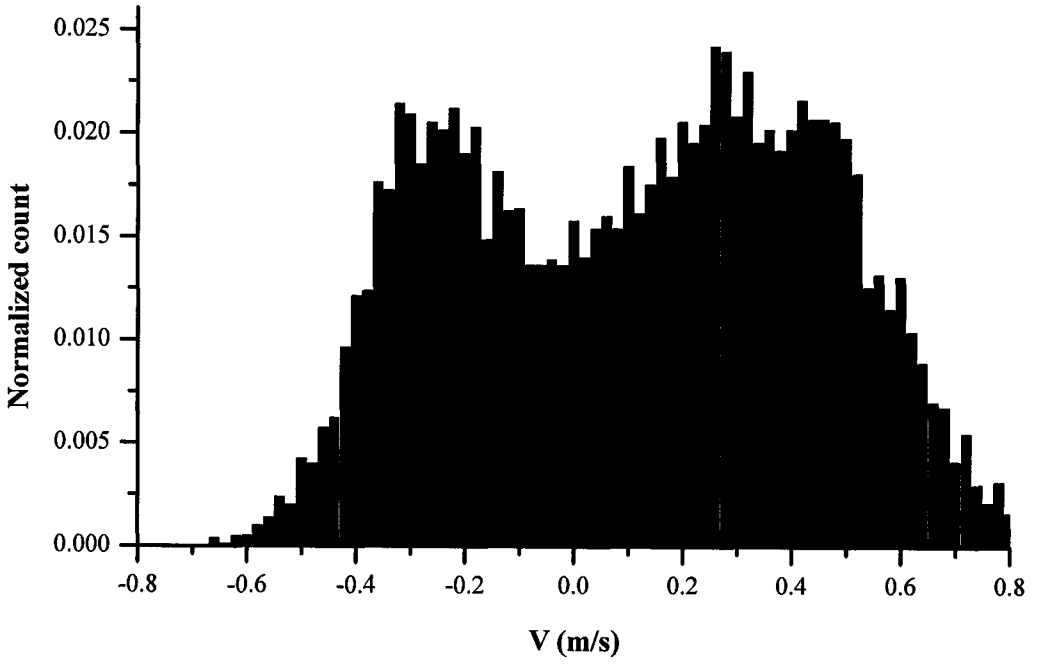

Figure 4-10: Velocity histogram at the bottom of scour hole for $y_t/b_o = 20$

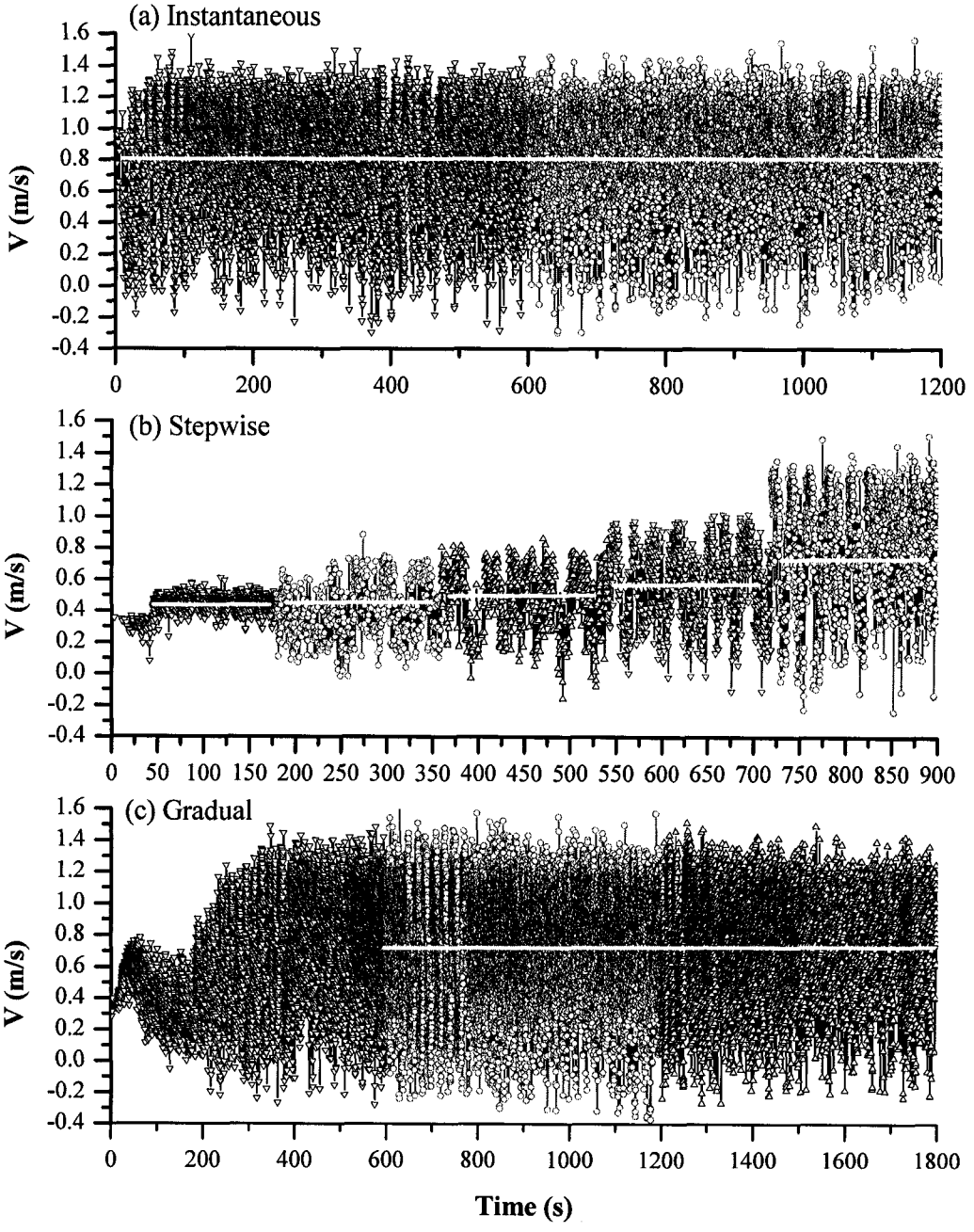

Figure 4-11: Effect of test startup conditions for $y_t/b_o = 4$

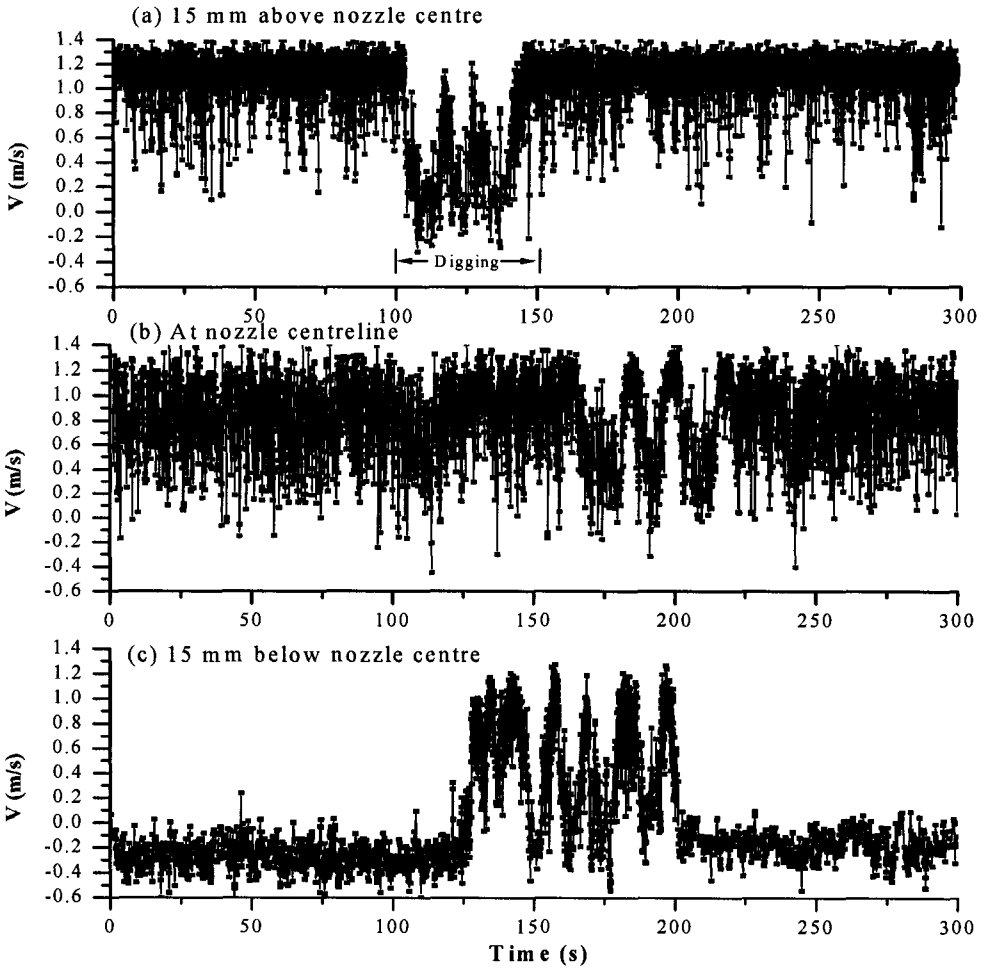

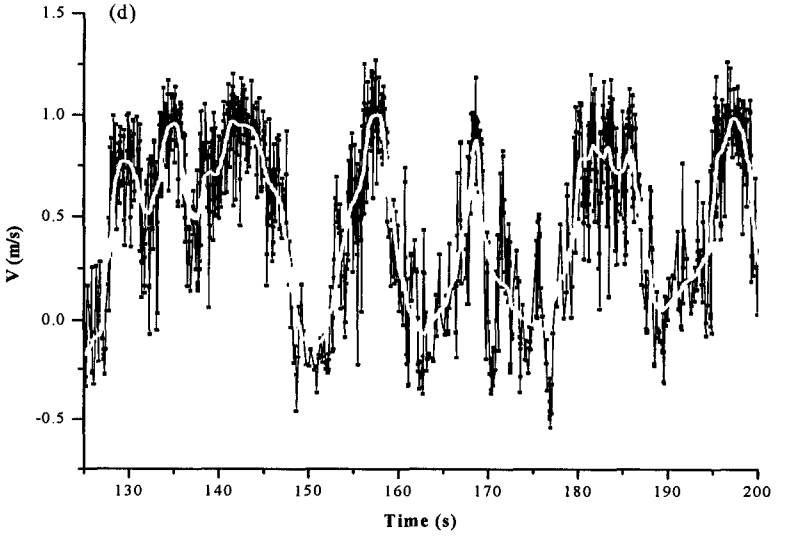

Figure 4-12: Digging and refilling phases for $y_t/b_o = 4$

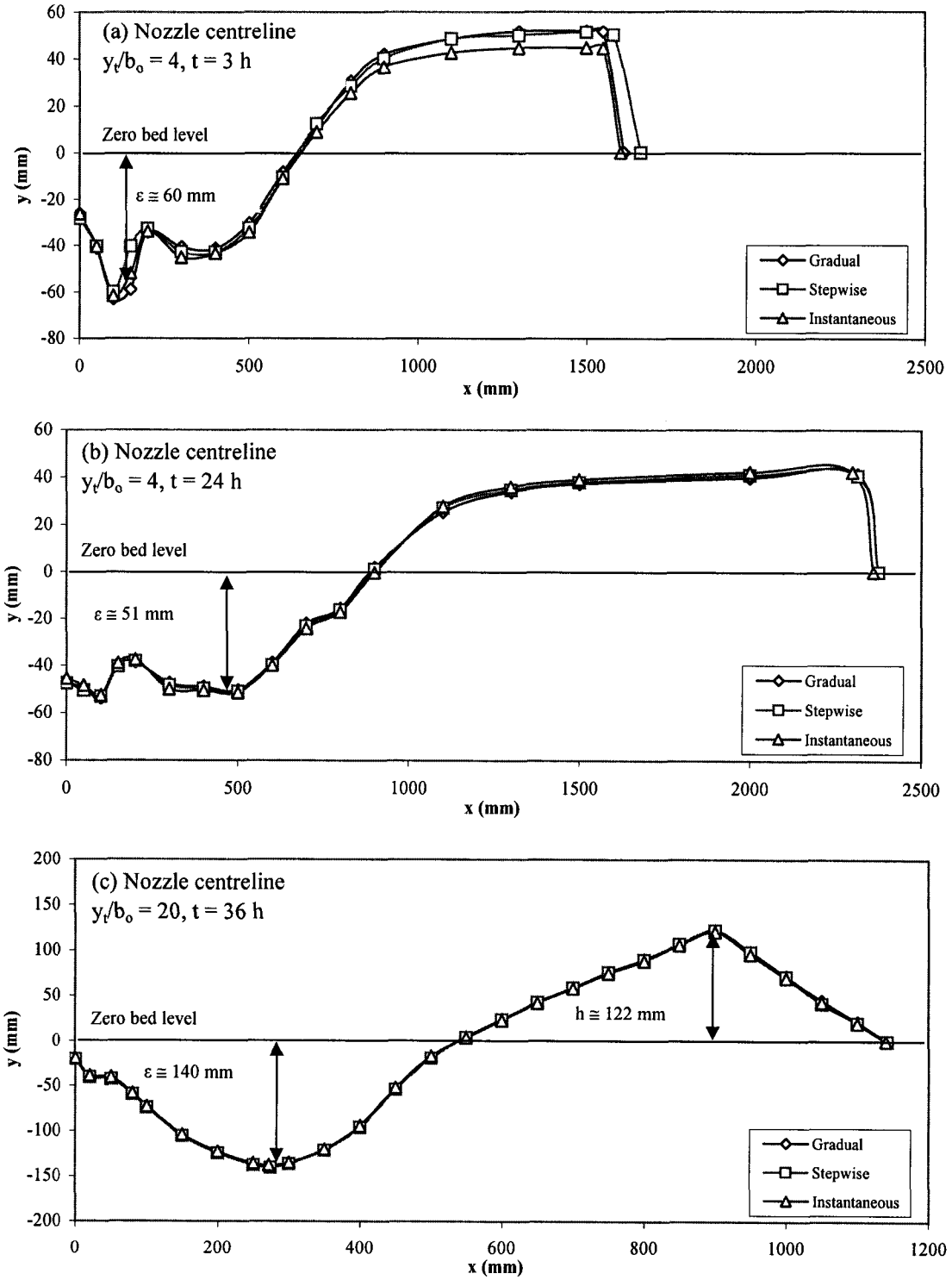

Figure 4-13: Effects of test startup conditions on the scour profiles

(a) Nozzle centreline @ x = $3b_o$

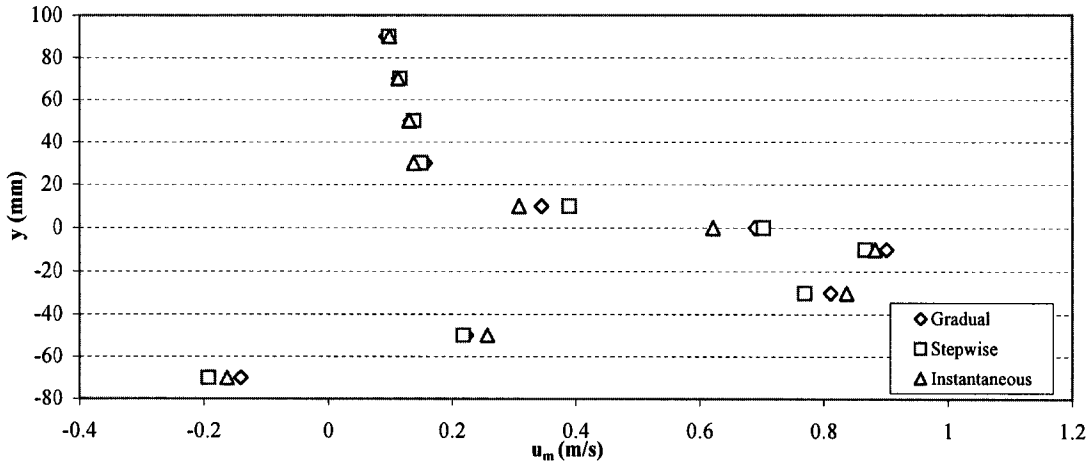

(b) Nozzle centreline @ start of mound

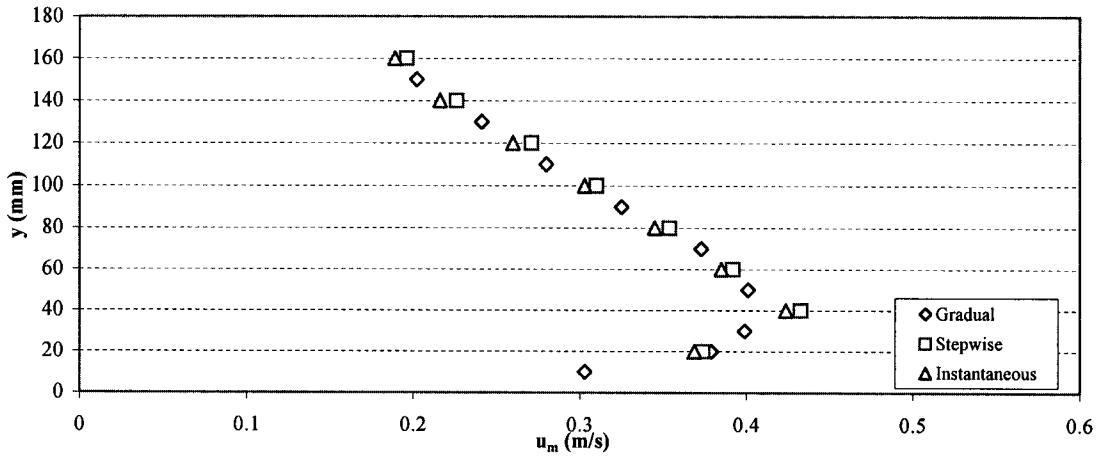

(c) Nozzle centreline @ top of mound

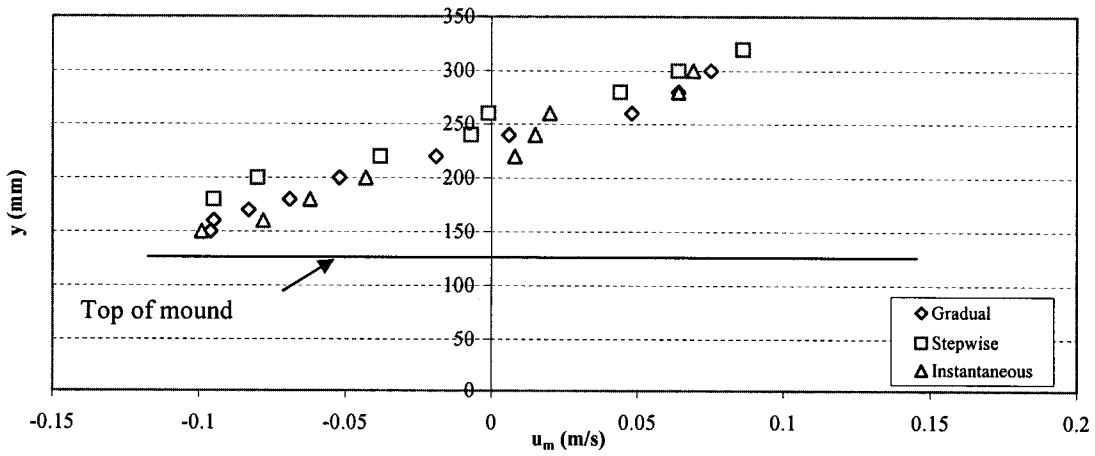

Figure 4-14: Velocity profiles along nozzle centreline for different startup conditions at $y_t/b_o = 20$

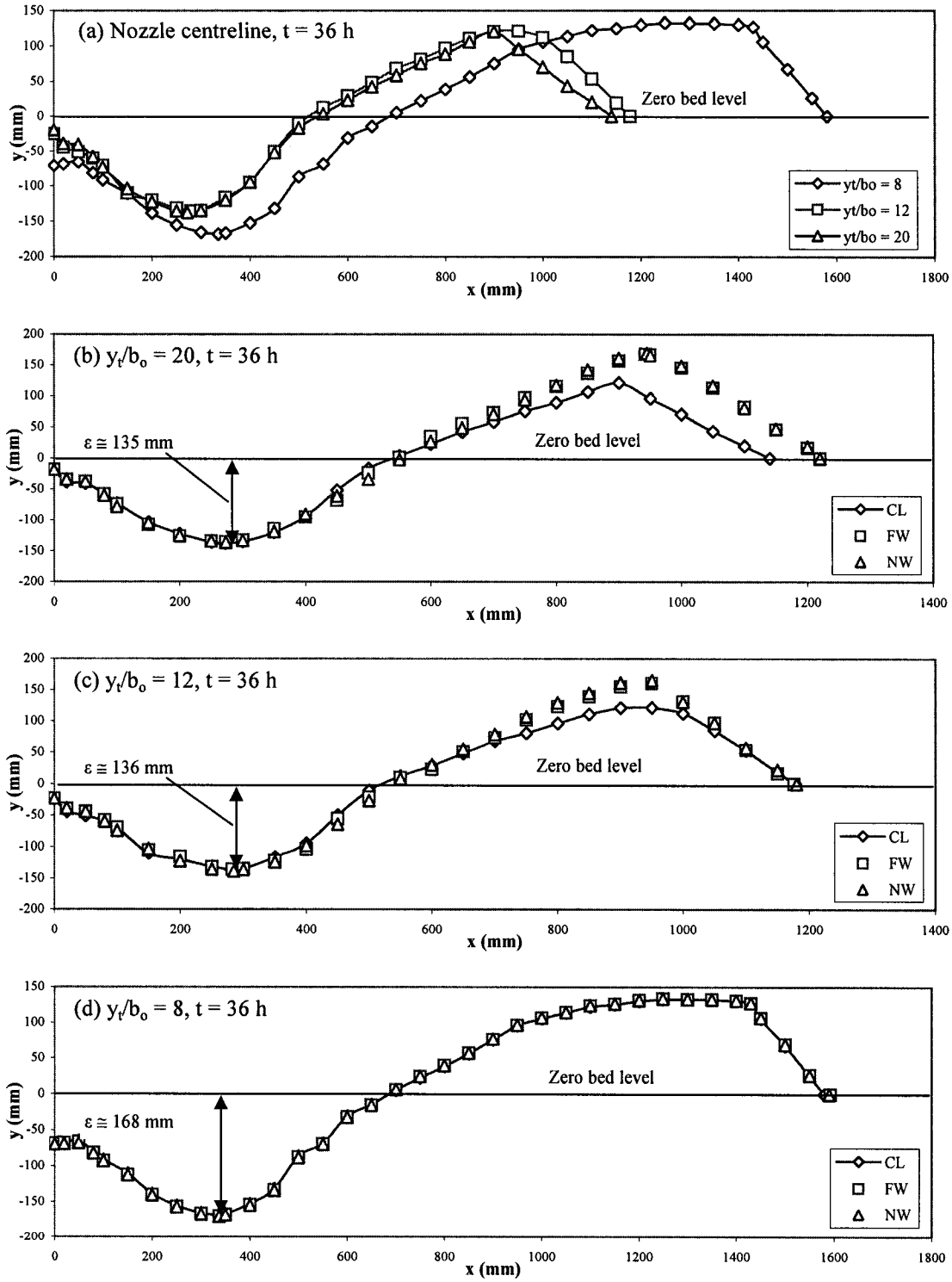

Figure 4-15: Scour hole profiles at different x-stations for higher submergences

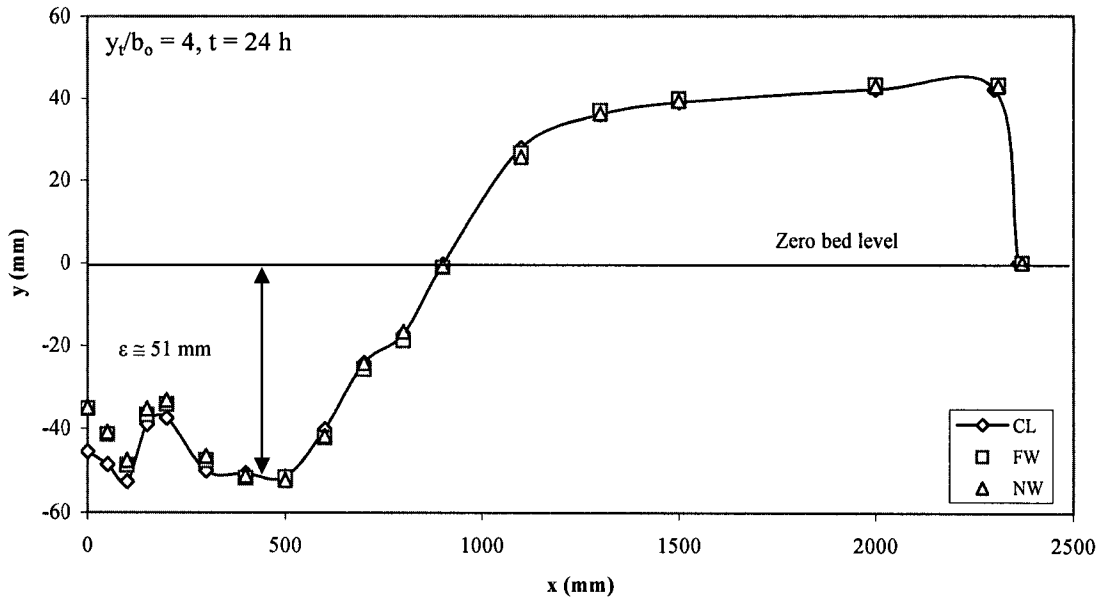

Figure 4-16: Scour hole profiles at different x-stations for lowest submergence

(a) $y_t/b_o = 20$ @ t = 24 h

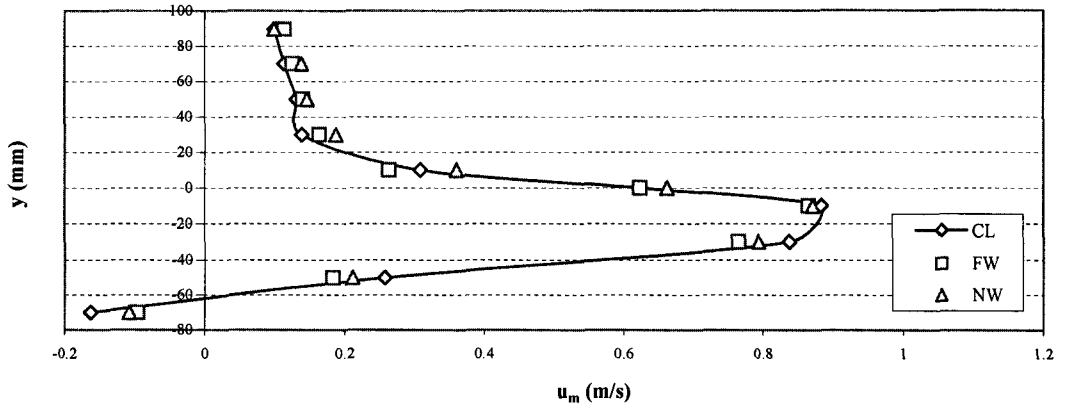

(b) $y_t/b_o = 12$ @ t = 24 h

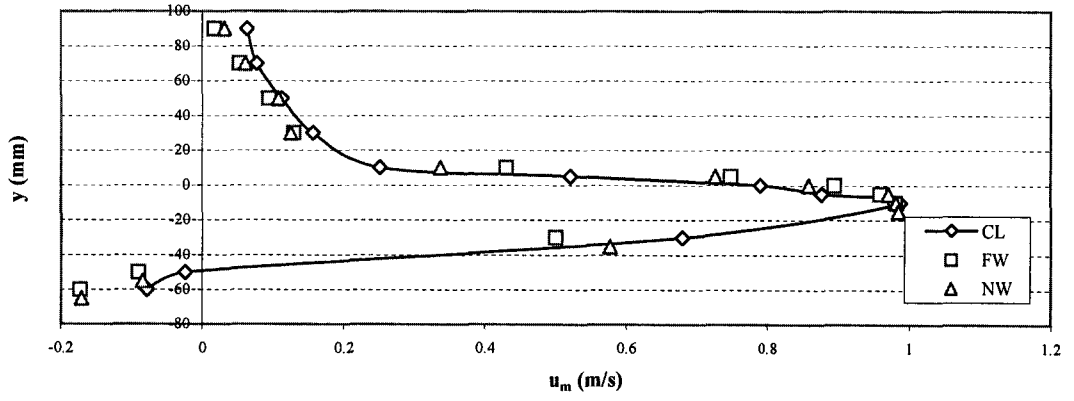

(c) $y_t/b_o = 8$ @ t = 24 h

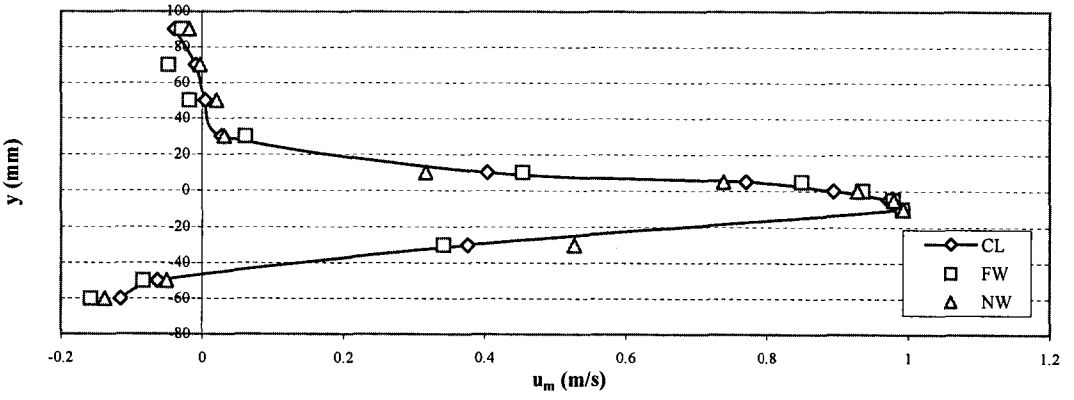

Figure 4-17: Velocity profiles at $x=3b_o$ for deeper submergences at different x-stations

(a) $y_t/b_o = 20$ @ t = 27 h

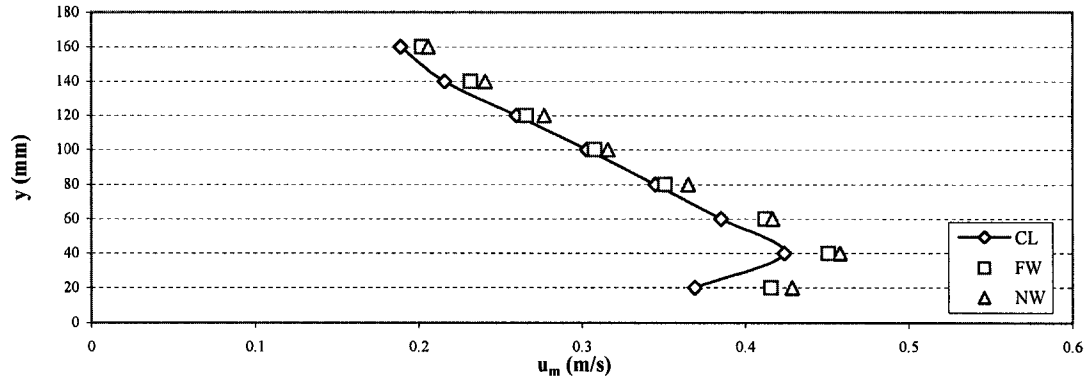

(b) $y_t/b_o = 12$ @ t = 27 h

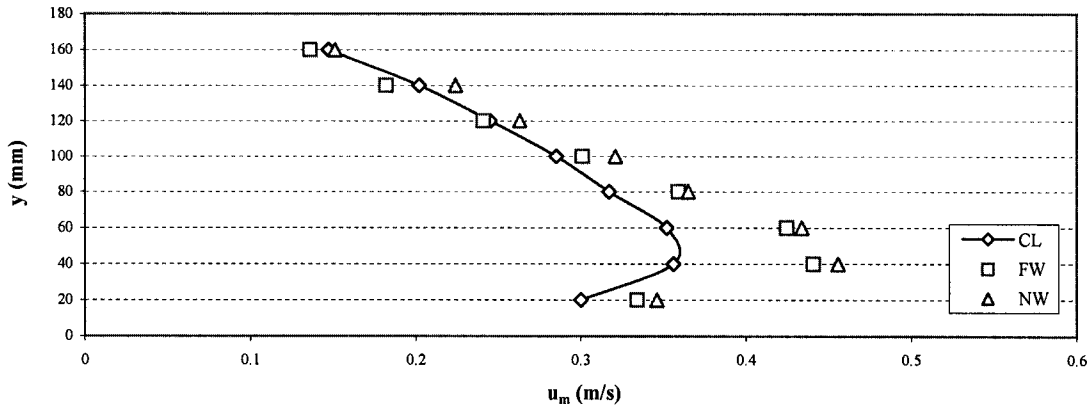

(c) $y_t/b_o = 8$ @ t = 27 h

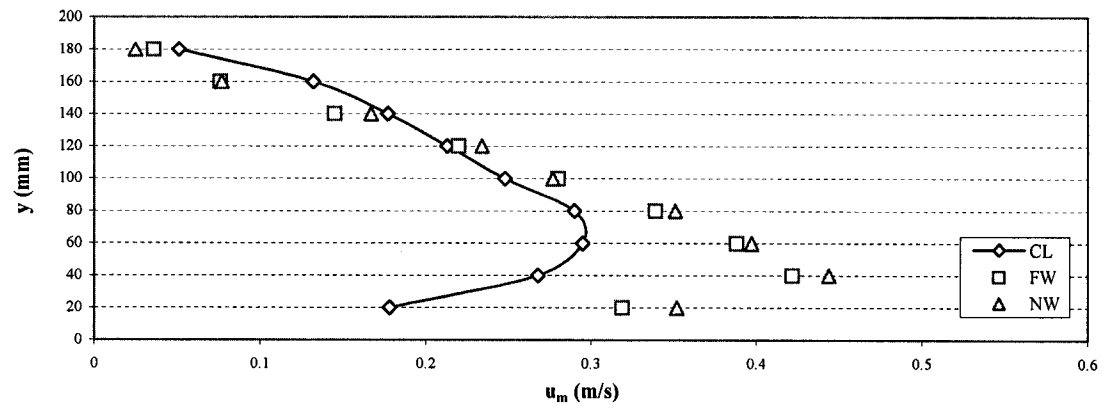

Figure 4-18: Velocity profiles at start of mound for deeper submergences at different x-stations

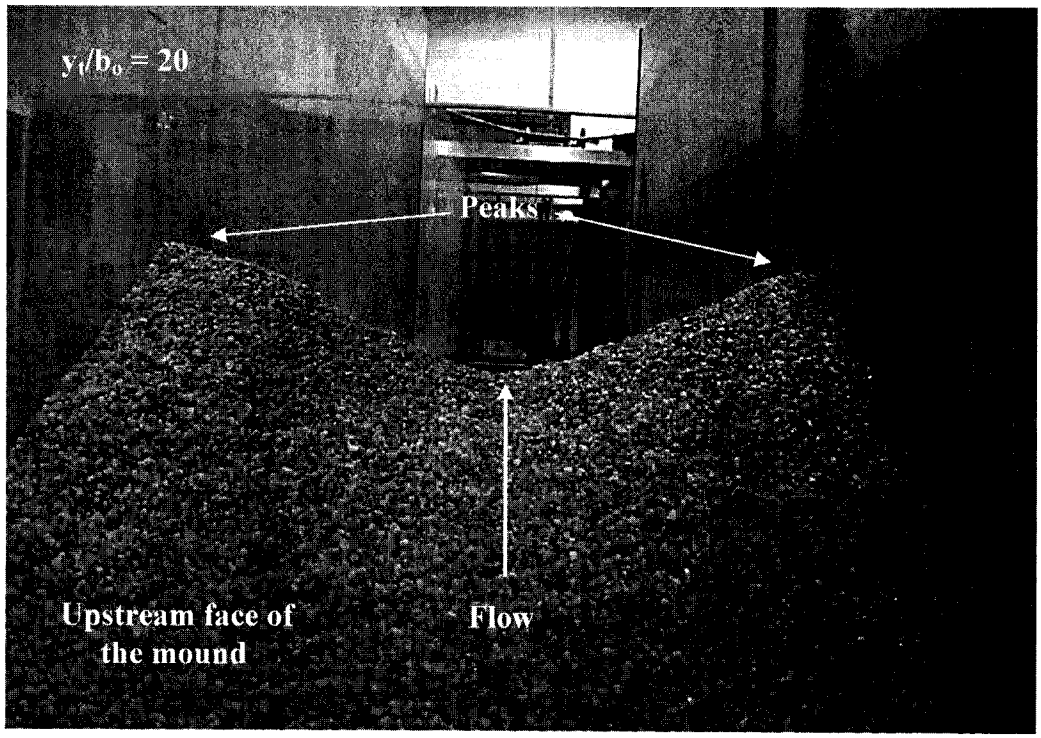

Figure 4-19: View of the mound region as seen from the nozzle

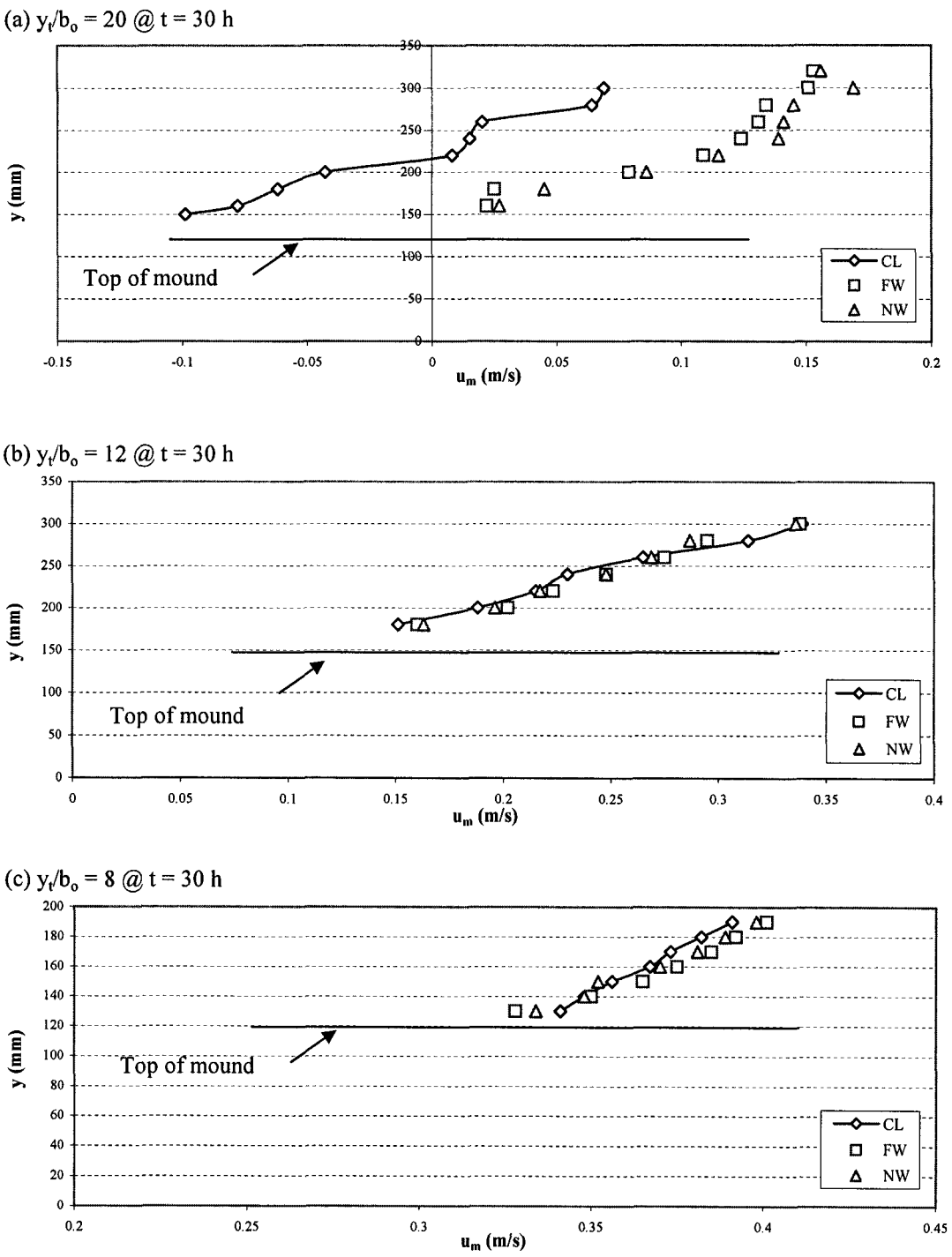

Figure 4-20: Velocity profiles at top of mound for varying submergence at different x-stations

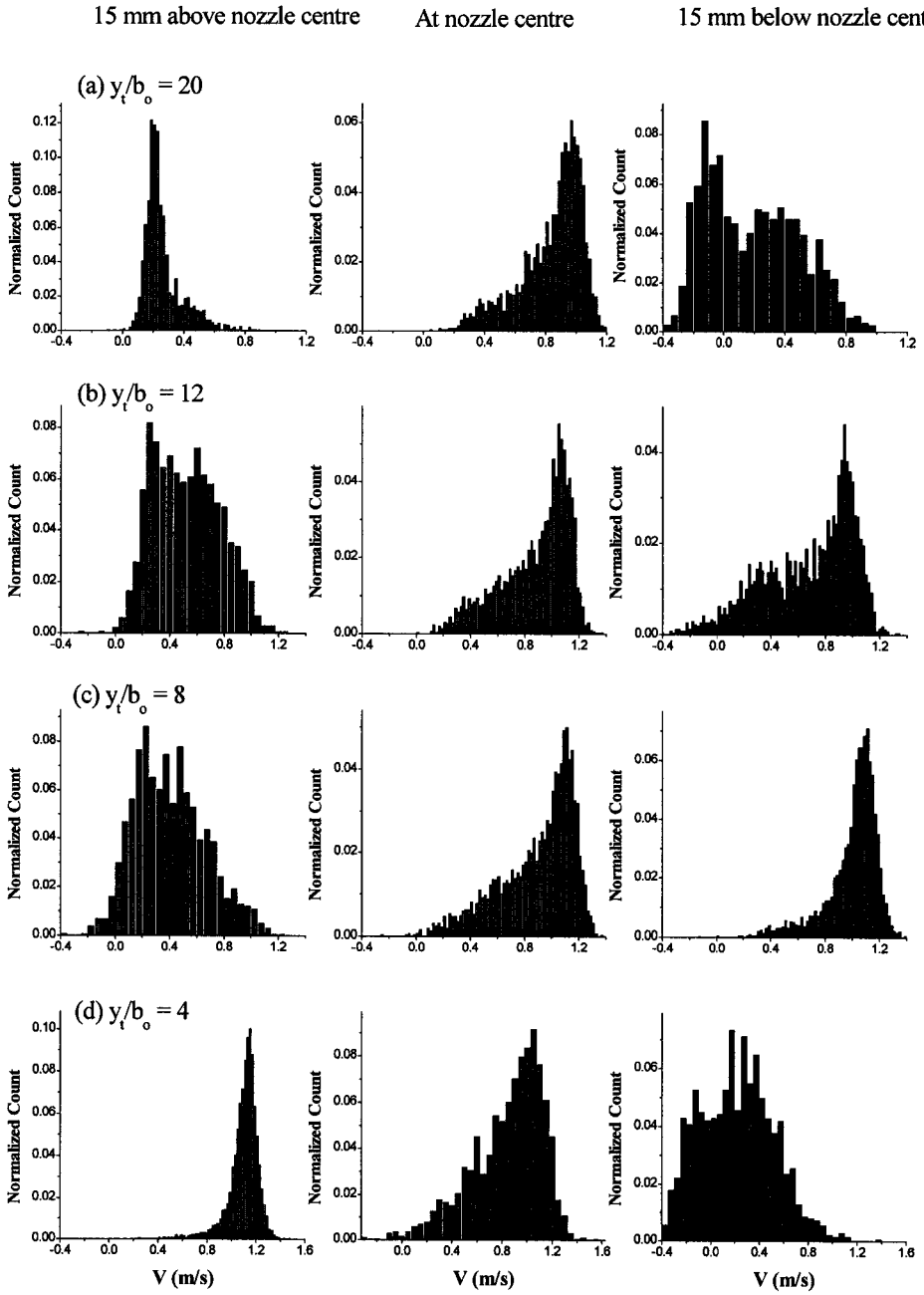

Figure 4-21: Velocity histograms for all submergences

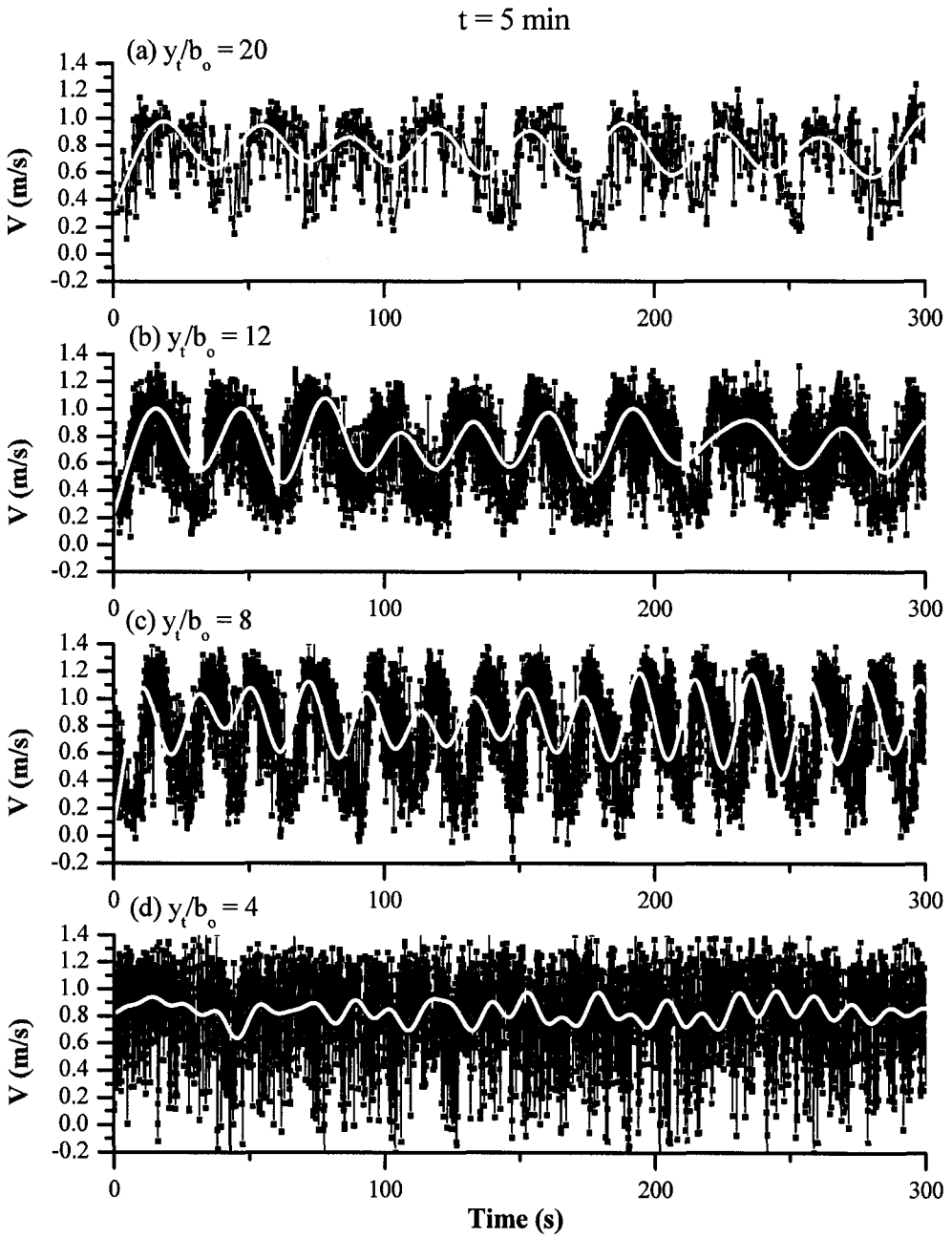

Figure 4-22: Velocity data showing effect of submergence at start of test

CHAPTER 5: CONCLUSIONS AND RECOMMENDATIONS

5.1 Conclusions

The present study carried out over a range of submergences indicates that there are two distinct types of flow fields, one at lower and other at higher submergences. Qualitatively, the observations are similar to that noticed in previous studies. The present velocity measurements confirm that there is the distinct flicking of the jet from the bed region towards the free surface in case of lower submergences. At higher submergences, the impingement point tends to move longitudinally forwards and backwards over a very wide region. The velocity observations confirm that this movement is more rapid with decreasing submergence. It should be noted in the present study, the flow at $y_t/b_o = 8$ resembles that of a jet at high submergence and is contrary to earlier observations (e.g. Balachandar et al., 2000; Kells et al., 2001) where the flow showed the presence of alternating flow fields that occurs at low submergences. The demarcation between low and high submergence depends on several factors and is worthy of further investigation.

The effects of startup conditions linger on for some time after the required test velocity is attained as noticed from the velocity measurements. However, the scour profiles are influenced for a longer period of time and one can notice differences up to a period of three hours. Beyond 24 hours one cannot distinguish any significant differences in both velocity and scour profiles. With increasing time, the low pass filtered data indicates no significant changes in the flow field characteristics after about 6 hours.

The scour profiles indicate that there are variations in the mound region, which is dependent on the level of submergence. Though flow visualization indicates that the flow fields are nominally similar at the three higher tailwater depths, certain distinctions can

be found as indicated by the velocity measurements. In the region close to the nozzle, no variations in velocity profiles were noted in the present study indicating that the lateral distribution of jet momentum was constant. Though variations were noted at farther distances from the nozzle, these variations were symmetrical about the jet axis. Non-symmetrical scour profile variations similar to that noted in previous studies, were not distinguished in this work. Any cross-sectional scour profile variations conform to changes in the velocity profiles. Together with the velocity measurements, the present profile measurements provide new insights into the mechanism of jet scour.

5.2 Recommendations for future work

On the basis of the above conclusions and our current understanding of the interaction of plane turbulent wall jets with a moveable boundary, the following recommendations are relevant for future work

There have been conflicting results regarding the lower submergence with some studies observing the jet flicking phenomenon at a particular value of lower submergence while some studies have not observed this phenomenon at the same value of submergence. Hence there is a need for closer investigation of the demarcation of lower and deep submergence along with other factors that might influence the jet movement at lower submergences.

This study made an attempt to vary the test startup conditions and study their effects on the scour mechanism and scour profiles. It would be interesting to vary the tailwater during the experiment by rising or lowering the tailwater and analyzing the effects on the jet movement.

This study has noted some interesting observations regarding the variability across the channel width, which has not been reported by many previous studies. It is therefore recommended to carry out experiments by varying the channel width to further understand and investigate the reasons for these three-dimensional effects caused by flows that are nominally two-dimensional.

REFERENCES

Aderibigbe, O., and Rajaratnam, N. (1998). "Effect of sediment gradation on erosion by plane turbulent wall jets." *Journal of Hydraulic Engineering*, ASCE, 124(10), 1034-1042.

Ahsan, Md.R. (2003). "Submergence effects on local scour," MASc thesis, University of Windsor, Windsor, Ontario, Canada.

Ahsan, Md. R., and Mazurek, K. (2003). "Submergence effects on interaction of flow with the sediment bed in local scour." *Proceedings of the 31st Annual Conference of the Canadian Society for Civil Engineering*, Moncton, New Brunswick, Canada, Paper No. GLC-275.

Ali, K.H.M., and Lim, S.Y. (1986). "Local scour caused by submerged wall jets." *Proceedings of Institution of Civil Engineers*, Part 2, 81, 607-645.

Ali, K.H.M., and Salehi Neyshaboury, A.A. (1991). "Localized scour downstream of a deeply submerged horizontal jet." *Proceedings of the Institution of Civil Engineers*, Part 2, 91, 1-18.

Balachandar, R., and Kells, J.A. (1997). "Local channel scour in uniformly graded sediments: the time-scale problem." *Canadian Journal of Civil Engineering*, 24(5), 799-807.

Balachandar, R., Kells, J.A., and Thiessen, R.J. (2000). "The effect of tailwater depth on the dynamics of local scour." *Canadian Journal of Civil Engineering*, 27(1), 138-150.

Breusers, H.N.C., and Raudkivi, A.J. (1991). *Scouring*. Hydraulic Structures Design Manual 2, International Association for Hydraulic Research, A.A. Balkema, Rotterdam, The Netherlands, 143p.

Chatterjee, S.S., and Ghosh, S.N. (1980). "Submerged horizontal jet over erodible bed." *Journal of Hydraulic Division*, ASCE, 106(HY11), 1765-1782.

Chatterjee, S.S., Ghosh, S.N., and Chatterjee, M. (1994). "Local scour due to submerged horizontal jet." *Journal of Hydraulic Engineering*, ASCE, 120(8), 973-993.

Coleman, H.W., and Steele, W.G. (1999). *Experimentation and Uncertainty Analysis for Engineers*, John Wiley and Sons, New York, USA, 275p.

Ead, S.A., and Rajaratnam, N. (2002). "Plane turbulent wall jets in shallow tailwater." *Journal of Engineering Mechanics*, ASCE, 128(2), 143-155.

Eaton, J.K., and Johnston, J.P. (1981). "A review of research on subsonic turbulent flow reattachment." *AIAA Journal*, 1093-1100.

Hussein, H.J, Capp, S.P., and George, W. K. (1994). "Velocity measurements in a high-Reynolds number, momentum-conserving, axisymmetric, turbulent jet." *Journal of Fluid Mechanics*, 258, 31-75.

Johnston, A.J., Volker, R.E., and Halliwell, A.R. (1987). "Scourhole developments in shallow tailwaters." *Conference on Hydraulics in Civil Engineering*, Melbourne, Australia, 162-166.

Johnston, A.J. (1990). "Scourhole developments in shallow tailwater." *Journal of Hydraulic Research*, 28(3), 341-354.

Karim, O.A., and Ali, K.H.M. (2000). "Prediction of flow patterns in local scour holes caused by turbulent water jets." *Journal of Hydraulic Research*, 38(4), 279-287.

Karlsson, R.I., Eriksson, J., and Persson J. (1992). "LDV measurements in a plane wall jet in a large enclosure." *6th International Symposium on Applications of Laser Techniques to Fluid Mechanics*, Lisbon, Portugal, Paper No. 1:5.

Kells, J.A., Balachandar, R., and Hagel, K.P. (2001). "Effect of grain size on local channel scour below a sluice gate." *Canadian Journal of Civil Engineering*, 28, 440-451.

Laursen, E.M. (1952). "Observations on the nature of scour." *Proceedings of the 5th Hydraulic Conference*, Bulletin 34, State University of Iowa, 179-197.

Mazurek, K. (2001). "Scour of clay by jets." PhD thesis, University of Alberta, Edmonton, Alberta, Canada.

Moffat, R.J. (1988). "Describing the uncertainties in experimental results." *Experimental Thermal and Fluid Science*, 1, 3-17.

Mohamed, M.S. (1990). "Erosion prediction and control in irrigation canals," PhD thesis, University of Windsor, Windsor, Ontario, Canada.

Mohamed, M.S., and McCorquodale, J.A. (1992). "Short-term local scour." *Journal of Hydraulic Research*, 30(5), 685-699.

Nik Hassan, N.M.K., and Narayanan, R. (1985). "Local scour downstream of an apron." *Journal of Hydraulic Engineering*, ASCE, 111(11), 1371-1385.

Rajaratnam, N. (1965a). "Submerged hydraulic jump." *Journal of the Hydraulic Division, Proceedings of the American Society of Civil Engineers*, 91(HY4), 71-76.

Rajaratnam, N. (1965b). "The hydraulic jump as a wall jet." *Journal of the Hydraulic Division, Proceedings of the American Society of Civil Engineers*, 91(HY5) 107-132.

Rajaratnam, N. (1976). *Turbulent jets*. Elsevier Scientific Publishing Company, Amsterdam, 304p.

Rajaratnam, N. (1981). "Erosion by plane turbulent jets." *Journal of Hydraulic Research*, 19(4), 339-358.

Rajaratnam, N., and Macdougall, R. K. (1983). "Erosion by plane wall jets with minimum tailwater." *Journal of Hydraulic Engineering*, ASCE, 109(7), 1061-1064.

Rouse, H. (1939). "A criteria for similarity in the transportation of sediment," *Proceedings of the 1st Hydraulic Conference*, Bulletin 20, State University of Iowa, Iowa City, Iowa, 33-49.

Tachie, M.F. (2001). "Open channel turbulent boundary layers and wall jets on rough surfaces." PhD thesis, Dept. of Civil and Geological Engineering, University of Saskatchewan, Saskatoon, Saskatchewan, Canada.

Tarapore, Z.S. (1956). "Scour below a submerged sluice gate," MSc Thesis, Dept. of Civil Engineering, University of Minnesota, Minneapolis, Minnesota, USA.

Topping, J. (1957). *Errors of observation and their treatment*. The Institute of Physics, London, 119p.

Venas, B., Abrahamsson, H., Krogstad, P.A., and Lofdahl, L. (1999). "Pulsed hot-wire measurements in two- and three-dimensional wall jets." *Experiments in Fluids*, 27, 210-218.

Wu, S., and Rajaratnam, N. (1995). "Free jumps, submerged jumps and wall jets." *Journal of Hydraulic Research*, 33(2), 197-212.

Wygnanski, I., Katz, Y., and Horev, E. (1992). "On the applicability of various scaling laws to the turbulent wall jet." *Journal of Fluid Mechanics*, 234, 669-690.

APPENDIX A

COMPARISON OF EMPIRICAL SCOUR PREDICTION FORMULAE

Table A-1: Empirical formulae for maximum scour depth

	Maximum scour depth, ε_m		
F_o	Equation used	Computed ε_m/b_o	Actual ε_m/b_o (Present study)
6.2	Eq. A-1	4.2	5.4
6.2	Eq. A-2	6.7	5.4
6.2	Eq. A-3	7.4	5.4

Table A-2: Empirical formula for maximum mound height

	Maximum mound height, Δ		
F_o	Equation used	Computed Δ/b_o	Actual Δ/b_o (Present study)
6.2	Eq. A-4	8	4.8

Eq. A-1: For $F_o < 12$, $\frac{\varepsilon_m}{b_o} = 0.04[F_o\left(\frac{y_t}{b_o}\right)^{0.1}]^2 + 0.08[F_o\left(\frac{y_t}{b_o}\right)^{0.1}] + 0.71$ (Ahsan, 2003)

Eq. A-2: $\frac{\varepsilon_m}{b_o} = (\tan\Phi)^{0.5}\left(\frac{d_{50}}{b_o}\right)^{0.25} F_0^{1.5}$ (Breusers and Raudkivi, 1991)

where, Φ is the angle of repose of the sand.

Eq. A-3: $\frac{\varepsilon_m}{b_o} = 2.3\left(\frac{U_o}{w}\right)^{\frac{1}{2}}\left(\frac{d_{50}}{b_o}\right)^{\frac{3}{8}} F_o^{\frac{3}{4}} - 1.19$ (Ali and Lim, 1986)

where, w is the fall velocity of the sand.

Eq. A-4: $\frac{\Delta}{b_o} = 2.5(F_o - 3)$ (Rajaratnam, 1981)

APPENDIX B

SCOUR HOLE PROFILE DATA

TEST A

Startup condition:	Gradual		Jet velocity (U_o):	1.16	m/s
Δh (manometer) =	9.2	cm	Tailwater depth (y_t):	101	mm
Submergence (y_t/b_o):	4		Nozzle opening (b_o):	25.4	mm
Sand size (D_{50}) (mm):	2.15		Duration of test:	3	h

Far Wall (FW)		Centreline (CL)		Near Wall (NW)	
x (mm)	ε_{FW} (mm)	x (mm)	ε_{CL} (mm)	x (mm)	ε_{NW} (mm)
0	-19.25	0	-26.12	0	-19.06
50	-38.16	50	-41.09	50	-37.81
100	-59.38	100	-63.01	100	-58.62
150	-58.07	150	-59.03	150	-57.24
200	-36.19	200	-34.26	200	-35.45
300	-42.24	300	-40.72	300	-40.86
400	-42.88	400	-41.32	400	-41.68
500	-32.41	500	-30.22	500	-30.77
600	-9.56	600	-8.43	600	-8.91
700	12.12	700	11.14	700	11.52
800	32.04	800	30.57	800	30.95
900	43.55	900	41.8	900	42.43
1100	50.64	1100	48.52	1100	48.79
1300	53.71	1300	51.71	1300	51.52
1500	53.86	1500	51.82	1500	51.74
1565	53.69	1550	51.6	1563	51.6
1625	0	1610	0	1624	0

TEST A

Startup condition:	Gradual		Jet velocity (U_o):	1.16	m/s
Δh (manometer) =	9.2	cm	Tailwater depth (y_t):	101	mm
Submergence (y_t/b_o):	4		Nozzle opening (b_o):	25.4	mm
Sand size (D_{50}) (mm):	2.15		Duration of test:	24	h

Far Wall (FW)		Centreline (CL)		Near Wall (NW)	
x (mm)	ε_{FW} (mm)	x (mm)	ε_{CL} (mm)	x (mm)	ε_{NW} (mm)
0	-36.24	0	-47.06	0	-35.82
50	-42.63	50	-49.87	50	-41.12
100	-49.88	100	-53.74	100	-47.36
150	-38.22	150	-40.13	150	-37.08
200	-35.77	200	-38.68	200	-34.43
300	-46.18	300	-47.59	300	-45.52
400	-50.16	400	-49.02	400	-49.95
500	-51.87	500	-50.45	500	-51.79
600	-40.34	600	-38.88	600	-40.01
700	-24.03	700	-22.17	700	-23.62
800	-17.08	800	-15.64	800	-16.25
900	1.13	900	1.87	900	1.07
1100	24.66	1100	25.49	1100	23.88
1300	34.51	1300	33.86	1300	34.06
1500	39.15	1500	37.13	1500	38.74
2000	41.44	2000	39.71	2000	40.53
2320	41.11	2315	41.25	2320	40.29
2385	0	2375	0	2385	0

TEST B

Startup condition:	Stepwise		Jet velocity (U_o):	1.16	m/s
Δh (manometer) =	9.2	cm	Tailwater depth (y_t):	101	mm
Submergence (y_t/b_o):	4		Nozzle opening (b_o):	25.4	mm
Sand size (D_{50}) (mm):	2.15		Duration of test:	3	h

Far Wall (FW)		Centreline (CL)		Near Wall (NW)	
x (mm)	ε_{FW} (mm)	x (mm)	ε_{CL} (mm)	x (mm)	ε_{NW} (mm)
0	-20.59	0	-28.23	0	-20.03
50	-40.06	50	-40.31	50	-38.84
100	-56.38	100	-59.98	100	-54.69
150	-38.64	150	-40.39	150	-35.12
200	-30.25	200	-32.62	200	-28.98
300	-44.66	300	-42.7	300	-45.08
400	-46.98	400	-42.83	400	-45.74
500	-35.57	500	-32.34	500	-34.31
600	-12.45	600	-10.49	600	-11.25
700	14.16	700	12.5	700	12.65
800	30.3	800	28.62	800	28.88
900	41.87	900	40.14	900	40.51
1100	48.65	1100	48.53	1100	46.63
1300	50.44	1300	49.95	1300	49.11
1500	50.61	1500	51.37	1500	49.53
1590	50.5	1580	50.14	1588	49.34
1670	0	1660	0	1670	0

TEST B

Startup condition:	Stepwise		Jet velocity (U_o):	1.16	m/s
Δh (manometer) =	9.2	cm	Tailwater depth (y_t):	101	mm
Submergence (y_t/b_o):	4		Nozzle opening (b_o):	25.4	mm
Sand size (D_{50}) (mm):	2.15		Duration of test:	24	h

Far Wall (FW)		Centreline (CL)		Near Wall (NW)	
x (mm)	ε_{FW} (mm)	x (mm)	ε_{CL} (mm)	x (mm)	ε_{NW} (mm)
0	-35.63	0	-47.7	0	-35.07
50	-42.15	50	-50.64	50	-41.53
100	-49.2	100	-53.18	100	-47.94
150	-37.36	150	-40.49	150	-36.69
200	-34.95	200	-38.15	200	-34.12
300	-46.84	300	-48.34	300	-45.83
400	-50.74	400	-49.81	400	-50.28
500	-51.21	500	-51.03	500	-52.44
600	-41.18	600	-39.88	600	-41.05
700	-24.67	700	-23.16	700	-25.11
800	-17.88	800	-16.27	800	-17.46
900	1.4	900	1.13	900	1.29
1100	25.55	1100	27.11	1100	24.65
1300	35.31	1300	34.52	1300	34.87
1500	40.05	1500	37.77	1500	39.54
2000	41.71	2000	40.85	2000	41.22
2320	41.42	2315	40.56	2320	41.08
2380	0	2375	0	2380	0

TEST C

Startup condition:	Instantaneous		Jet velocity (U_o):	1.16	m/s
Δh (manometer) =	9.2	cm	Tailwater depth (y_t):	101	mm
Submergence (y_t/b_o):	4		Nozzle opening (b_o):	25.4	mm
Sand size (D_{50}) (mm):	2.15		Duration of test:	3	h

Far Wall (FW)		Centreline (CL)		Near Wall (NW)	
x (mm)	ε_{FW} (mm)	x (mm)	ε_{CL} (mm)	x (mm)	ε_{NW} (mm)
0	-20.11	0	-26.15	0	-20.62
50	-38.69	50	-40.35	50	-39.64
100	-58.81	100	-61.54	100	-59.16
150	-49.56	150	-51.81	150	-49.81
200	-32.75	200	-33.86	200	-31.75
300	-46.48	300	-45.13	300	-45.59
400	-45.32	400	-43.3	400	-44.92
500	-36.07	500	-34.34	500	-36.53
600	-11.68	600	-10.96	600	-10.88
700	10.12	700	8.92	700	10.71
800	28.63	800	25.61	800	30.33
900	38.45	900	36.43	900	40.15
1100	44.11	1100	42.55	1100	45.64
1300	48.26	1300	44.57	1300	48.7
1500	48.71	1500	44.63	1500	48.96
1562	48.52	1550	44.5	1564	48.82
1613	0	1600	0	1615	0

TEST C

Startup condition:	Instantaneous		Jet velocity (U_o):	1.16	m/s
Δh (manometer) =	9.2	cm	Tailwater depth (y_t):	101	mm
Submergence (y_t/b_o):	4		Nozzle opening (b_o):	25.4	mm
Sand size (D_{50}) (mm):	2.15		Duration of test:	24	h

Far Wall (FW)		Centreline (CL)		Near Wall (NW)	
x (mm)	ε_{FW} (mm)	x (mm)	ε_{CL} (mm)	x (mm)	ε_{NW} (mm)
0	-35.15	0	-45.52	0	-34.9
50	-41.36	50	-48.51	50	-40.86
100	-48.68	100	-52.53	100	-47.48
150	-36.74	150	-38.97	150	-35.26
200	-34.17	200	-37.42	200	-33.14
300	-47.58	300	-49.99	300	-46.51
400	-51.67	400	-50.61	400	-51.13
500	-51.52	500	-51.37	500	-52.22
600	-42.11	600	-40.1	600	-41.77
700	-25.68	700	-24.23	700	-24.2
800	-18.89	800	-17.21	800	-16.68
900	-1.05	900	-0.35	900	-0.75
1100	26.56	1100	27.81	1100	25.63
1300	36.91	1300	35.9	1300	36.18
1500	39.87	1500	38.96	1500	39.27
2000	43.33	2000	42.16	2000	42.96
2310	43.21	2300	42.15	2310	42.89
2370	0	2360	0	2370	0

TEST D

Startup condition:	Instantaneous		Jet velocity (U_o):	1.16	m/s
Δh (manometer) =	9.2	cm	Tailwater depth (y_t):	203	mm
Submergence (y_t/b_o):	8		Nozzle opening (b_o):	25.4	mm
Sand size (D_{50}) (mm):	2.15		Duration of test:	72	h

Far Wall (FW)		Centreline (CL)		Near Wall (NW)	
x (mm)	ε_{FW} (mm)	x (mm)	ε_{CL} (mm)	x (mm)	ε_{NW} (mm)
0	-75.45	0	-75.91	0	-75.84
20	-74.51	20	-74.84	20	-74.79
50	-74.49	50	-74.33	50	-74.62
80	-83.12	80	-82.79	80	-83.64
100	-90.85	100	-90.6	100	-91.37
150	-119.38	150	-118.74	150	-119.59
200	-138.77	200	-138.25	200	-139.15
250	-155.11	250	-154.43	250	-155.93
300	-171.65	300	-171.26	300	-171.87
342	-179.35	340	-178.74	342	-179.21
350	-177.73	350	-176.19	350	-177.48
400	-165.14	400	-164.85	400	-165.07
450	-137.38	450	-136.95	450	-137.26
500	-104.87	500	-104.23	500	-105.01
550	-67.79	550	-67.09	550	-67.91
600	-45.68	600	-45.1	600	-45.88
650	-27.59	650	-27.18	650	-27.95
700	-5.9	700	-5.69	700	-6.13
750	11.08	750	10.57	750	11.58
800	29.32	800	28.65	800	29.61
850	45.15	850	44.91	850	45.45
900	66.17	900	65.62	900	66.29
950	85.33	950	84.74	950	85.41
1000	98.16	1000	97.57	1000	98.04
1050	110.22	1050	109.88	1050	110.1
1100	117.26	1100	116.85	1100	117.13
1150	121.84	1150	121.37	1150	121.56
1200	125.2	1200	124.51	1200	125.07
1250	127.66	1250	126.18	1250	127.22
1300	128.81	1300	127.71	1300	128.6
1350	128.93	1350	127.84	1350	128.81
1400	128.56	1400	128.23	1400	128.57
1450	128.69	1450	128.46	1450	128.44
1500	129.13	1500	129.06	1500	128.95
1515	124.1	1515	123.73	1515	124.03
1550	101.25	1550	100.87	1550	100.98
1600	68.36	1600	67.45	1600	68.14
1650	21.15	1650	20.08	1650	20.89
1685	0	1675	0	1685	0

TEST E

Startup condition:	Instantaneous		Jet velocity (U_o):	1.16	m/s
Δh (manometer) =	9.2	cm	Tailwater depth (y_t):	305	mm
Submergence (y_t/b_o):	12		Nozzle opening (b_o):	25.4	mm
Sand size (D_{50}) (mm):	2.15		Duration of test:	48	h

Far Wall (FW)		Centreline (CL)		Near Wall (NW)	
x (mm)	ε_{FW} (mm)	x (mm)	ε_{CL} (mm)	x (mm)	ε_{NW} (mm)
0	-25.39	0	-25.74	0	-24.71
20	-40.77	20	-45.62	20	-40.06
50	-45.6	50	-51.51	50	-45.65
80	-60.21	80	-62.13	80	-60.58
100	-70.95	100	-71.95	100	-75.91
150	-108.04	150	-111.39	150	-105.58
200	-116.66	200	-120.85	200	-123.22
250	-132.41	250	-131.91	250	-135.8
282	-136.1	280	-136.01	285	-138.61
300	-135.18	300	-135.12	300	-136.36
350	-122.52	350	-116.77	350	-124.97
400	-105.06	400	-95.69	400	-99.13
450	-55.75	450	-51.04	450	-65.87
500	-22.01	500	-11.4	500	-27.25
550	10.13	550	12.9	550	9.55
600	24.05	600	29.68	600	31.66
650	52.31	650	49.11	650	56.77
700	75.17	700	70.01	700	80.06
750	102.88	750	82.33	750	108.42
800	125.26	800	97.48	800	131.33
850	140.47	850	111.76	850	146.85
900	157.33	900	121.53	900	161.79
950	160.72	950	121.65	950	165.49
1000	132.26	1000	112.22	1000	131.26
1050	97.14	1050	84.88	1050	97.39
1100	53.96	1100	53.06	1100	57.33
1150	17.03	1150	18.21	1150	21.94
1176	0	1178	0	1180	0

TEST F

Startup condition:	Gradual		Jet velocity (U_o):	1.16	m/s
Δh (manometer) =	9.2	cm	Tailwater depth (y_t):	508	mm
Submergence (y_t/b_o):	20		Nozzle opening (b_o):	25.4	mm
Sand size (D_{50}) (mm):	2.15		Duration of test:	36	h

Far Wall (FW)		Centreline (CL)		Near Wall (NW)	
x (mm)	ε_{FW} (mm)	x (mm)	ε_{CL} (mm)	x (mm)	ε_{NW} (mm)
0	-19.06	0	-20.22	0	-18.86
20	-35.72	20	-40.08	20	-35.21
50	-38.11	50	-42.06	50	-39.04
80	-59.66	80	-59.09	80	-61.17
100	-75.15	100	-74.16	100	-79.62
150	-109.29	150	-105.2	150	-106.56
200	-127.46	200	-124.58	200	-125.09
250	-135.8	250	-137.63	250	-133.16
275	-137.15	273	-140.28	275	-135.03
300	-133.86	300	-136.02	300	-132.8
350	-115.1	350	-121.03	350	-120.18
400	-96.51	400	-95.58	400	-92.8
450	-69.21	450	-53.64	450	-63.08
500	-24.18	500	-18.85	500	-35.01
550	2.11	550	4.63	550	-1.9
600	36.47	600	24.16	600	28.31
650	56.41	650	43.52	650	50.8
700	73.97	700	59.42	700	71.68
750	97.4	750	76.59	750	93.63
800	116.64	800	90.67	800	116.25
850	138.88	850	108.12	850	140.58
900	158.7	900	122.8	900	160
950	169.61	950	99.09	950	170.02
1000	148.02	1000	72.28	1000	151.19
1050	114.72	1050	45.13	1050	118.91
1100	84.8	1100	21.44	1100	83.6
1150	48.6	1143	0	1150	50.28
1200	18.23			1200	20.09
1230	0			1230	0

TEST F

Startup condition:	Gradual		Jet velocity (U_o):	1.16	m/s
Δh (manometer) =	9.2	cm	Tailwater depth (y_t):	508	mm
Submergence (y_t/b_o):	20		Nozzle opening (b_o):	25.4	mm
Sand size (D_{50}) (mm):	2.15		Duration of test:	48	h

Far Wall (FW)		Centreline (CL)		Near Wall (NW)	
x (mm)	ε_{FW} (mm)	x (mm)	ε_{CL} (mm)	x (mm)	ε_{NW} (mm)
0	-19.69	0	-20.36	0	-19.03
20	-36.24	20	-40.51	20	-35.58
50	-38.95	50	-42.67	50	-39.37
80	-59.87	80	-59.35	80	-61.55
100	-75.48	100	-74.19	100	-79.7
150	-109.51	150	-105.33	150	-106.66
200	-127.63	200	-124.7	200	-125.17
250	-135.91	250	-137.72	250	-133.28
275	-137.22	273	-140.35	275	-135.11
300	-133.78	300	-136.16	300	-132.89
350	-115.27	350	-120.91	350	-120.21
400	-96.67	400	-95.41	400	-92.68
450	-69.46	450	-53.61	450	-62.97
500	-24.09	500	-18.88	500	-35.13
550	2.02	550	4.54	550	-1.99
600	36.38	600	24.02	600	28.23
650	56.5	650	43.65	650	50.71
700	74.09	700	59.59	700	71.76
750	97.58	750	76.76	750	93.75
800	116.75	800	90.81	800	116.36
850	138.97	850	108.26	850	140.7
900	158.82	900	122.93	900	160.22
950	169.9	950	99.21	950	170.15
1000	148.43	1000	72.36	1000	151.3
1050	114.88	1050	45.05	1050	119.08
1100	84.68	1100	21.36	1100	83.72
1150	48.48	1143	0	1150	50.19
1200	18.33			1200	19.98
1230	0			1230	0

TEST G

Startup condition:	Stepwise		Jet velocity (U_o):	1.16	m/s
Δh (manometer) =	9.2	cm	Tailwater depth (y_t):	508	mm
Submergence (y_t/b_o):	20		Nozzle opening (b_o):	25.4	mm
Sand size (D_{50}) (mm):	2.15		Duration of test:	36	h

Far Wall (FW)		Centreline (CL)		Near Wall (NW)	
x (mm)	ε_{FW} (mm)	x (mm)	ε_{CL} (mm)	x (mm)	ε_{NW} (mm)
0	-18.9	0	-20.65	0	-18.5
20	-34.96	20	-40.81	20	-34.91
50	-37.33	50	-42.74	50	-38.74
80	-57.81	80	-59.67	80	-60.6
100	-74.12	100	-74.59	100	-78.98
150	-108.52	150	-105.44	150	-106.71
200	-127.01	200	-124.68	200	-125.64
250	-135.1	250	-137.89	250	-133.58
276	-137.48	274	-140.7	276	-135.46
300	-134.09	300	-136.73	300	-133.02
350	-115.78	350	-121.55	350	-120.85
400	-97.14	400	-96.04	400	-93.37
450	-69.86	450	-54.11	450	-63.62
500	-24.65	500	-19.22	500	-35.49
550	3.03	550	4.16	550	-1.25
600	36.97	600	23.94	600	28.54
650	57.24	650	43.17	650	51.05
700	74.59	700	59.3	700	72.66
750	98.22	750	76.41	750	94.03
800	117.23	800	90.07	800	116.89
850	139.51	850	107.89	850	141.2
900	159.98	900	122.48	900	161.1
950	170.16	950	98.82	950	170.85
1000	148.67	1000	71.75	1000	152.13
1050	115.35	1050	41.69	1050	119.32
1100	85.42	1100	20.18	1100	84.28
1150	51.06	1142	0	1150	50.15
1200	20.4			1200	19.92
1230	0			1230	0

TEST G

Startup condition:	Stepwise		Jet velocity (U_o):	1.16	m/s
Δh (manometer) =	9.2	cm	Tailwater depth (y_t):	508	mm
Submergence (y_t/b_o):	20		Nozzle opening (b_o):	25.4	mm
Sand size (D_{50}) (mm):	2.15		Duration of test:	48	h

Far Wall (FW)		Centreline (CL)		Near Wall (NW)	
x (mm)	ε_{FW} (mm)	x (mm)	ε_{CL} (mm)	x (mm)	ε_{NW} (mm)
0	-19.81	0	-20.69	0	-18.62
20	-35.85	20	-40.98	20	-35.05
50	-37.97	50	-42.81	50	-38.88
80	-58.75	80	-69.61	80	-60.72
100	-74.69	100	-74.7	100	-79.14
150	-108.9	150	-105.56	150	-105.85
200	-127.16	200	-124.79	200	-125.76
250	-135.26	250	-137.96	250	-133.7
276	-137.58	274	-140.82	276	-135.54
300	-134.17	300	-136.8	300	-133.1
350	-115.9	350	-121.49	350	-120.92
400	-97.25	400	-96.13	400	-93.49
450	-69.95	450	-54.28	450	-63.72
500	-24.57	500	-19.38	500	-35.6
550	2.91	550	4.08	550	-1.31
600	37.11	600	23.82	600	28.48
650	57.38	650	43.26	650	50.96
700	74.7	700	59.44	700	72.77
750	98.35	750	76.56	750	94.15
800	117.36	800	70.21	800	117
850	139.65	850	107.98	850	141.33
900	160.11	900	122.6	900	161.22
950	170.25	950	98.91	950	170.97
1000	148.79	1000	71.82	1000	152.28
1050	115.47	1050	41.75	1050	119.4
1100	85.36	1100	20.1	1100	84.32
1150	50.92	1142	0	1150	50.08
1200	20.36			1200	19.86
1230	0			1230	0

TEST H

Startup condition:	Instantaneous		Jet velocity (U_o):	1.16	m/s
Δh (manometer) =	9.2	cm	Tailwater depth (y_t):	508	mm
Submergence (y_t/b_o):	20		Nozzle opening (b_o):	25.4	mm
Sand size (D_{50}) (mm):	2.15		Duration of test:	36	h

Far Wall (FW)		Centreline (CL)		Near Wall (NW)	
x (mm)	ε_{FW} (mm)	x (mm)	ε_{CL} (mm)	x (mm)	ε_{NW} (mm)
0	-18.71	0	-19.35	0	-18.11
20	-34.69	20	-38.78	20	-34.31
50	-37.84	50	-40.65	50	-37.96
80	-58.56	80	-57.95	80	-60.25
100	-74.08	100	-72.88	100	-78.51
150	-107.93	150	-103.59	150	-104.77
200	-126.18	200	-122.69	200	-125.64
250	-134.5	250	-135.7	250	-134.08
273	-135.9	272	-137.82	273	-136.12
300	-132.61	300	-135.13	300	-133.17
350	-114.28	350	-120.2	350	-118.81
400	-95.31	400	-94.44	400	-91.09
450	-67.98	450	-52.07	450	-61.22
500	-23.6	500	-16.96	500	-33.89
550	1.52	550	3.55	550	-2.35
600	34.87	600	22.86	600	26.65
650	55.04	650	42.09	650	48.74
700	72.66	700	58.34	700	70.59
750	96.45	750	75.17	750	93.61
800	115.27	800	88.88	800	117.06
850	136.89	850	106.35	850	141.88
900	156.75	900	121.08	900	161.07
942	167.8	950	95.97	944	169.3
950	166.91	1000	70.31	950	165.92
1000	145.38	1050	43.28	1000	148.26
1050	113.16	1100	20.05	1050	116.55
1100	82.4	1140	0	1100	80.78
1150	46.33			1150	47.63
1200	17.05			1200	18.64
1220	0			1220	0

TEST H

Startup condition:	Instantaneous		Jet velocity (U_o):	1.16	m/s
Δh (manometer) =	9.2	cm	Tailwater depth (y_t):	508	mm
Submergence (y_t/b_o):	20		Nozzle opening (b_o):	25.4	mm
Sand size (D_{50}) (mm):	2.15		Duration of test:	48	h

Far Wall (FW)		Centreline (CL)		Near Wall (NW)	
x (mm)	ε_{FW} (mm)	x (mm)	ε_{CL} (mm)	x (mm)	ε_{NW} (mm)
0	-19.6	0	-21.34	0	-19.2
20	-36.24	20	-40.01	20	-35.77
50	-39.88	50	-42.75	50	-39.45
80	-60.06	80	-58.59	80	-61.32
100	-76.59	100	-73.26	100	-79.88
150	-109.11	150	-105.1	150	-108.67
200	-127.34	200	-123.51	200	-127.02
250	-134.91	250	-136.02	250	-134.63
273	-135.98	272	-137.95	273	-136.24
300	-132.85	300	-135.47	300	-133.61
350	-115.67	350	-120.15	350	-119.77
400	-96.54	400	-95.35	400	-94.26
450	-69.41	450	-55.68	450	-64.45
500	-25.6	500	-18.5	500	-34.78
550	3.38	550	6.33	550	-2.52
600	36.49	600	27.19	600	28.33
650	57.22	650	46.2	650	51.54
700	74.24	700	62.43	700	72.27
750	98.25	750	78.42	750	95.18
800	116.91	800	92.63	800	117.25
850	138.07	850	111.56	850	142.65
900	157.26	900	121.21	900	161.46
942	167.92	950	93.92	944	169.41
950	167	1000	66.85	950	166.05
1000	145.78	1050	40.42	1000	147.81
1050	112.24	1100	19.77	1050	115.36
1100	80.88	1140	0	1100	78.97
1150	45.51			1150	46.03
1200	16.82			1200	18.15
1220	0			1220	0

APPENDIX C

ANALYSIS OF ERRORS AND UNCERTAINTY

This appendix provides an estimate of the errors and uncertainty in the different measured and derived quantities in the tests carried out in this study. The maximum errors are calculated thus denoting the worst case. The calculations used in estimating these errors are based on Topping (1957). The estimated errors are given in Table C-1.

A digital caliper with a precision of 0.01 mm was used for the nozzle measurement, which yields an estimated error in measurement of the nozzle opening thickness (b_o) of 0.04%. The tailwater depth (y_t) was measured using a measuring tape with the precision of 1 mm, thus the estimated error in y_t is 0.99%. The error for submergence (y_t/b_o), therefore, becomes 1.03%. The error in manometer reading, used for velocity measurements just outside the nozzle exit, can be 1 mm, which is the minimum unit of the manometer scale. This gives the maximum error in velocity measurement of 1.09%. Using these errors, the error in the derived flow Froude number (F_r) cane be estimated as 1.13%. Vertical dimensions pertaining to scour profile measurements in the tests were measured using an electronic point gauge of precision 0.01 mm. The estimated errors for maximum scour depth (ε_m) and maximum mound height (Δ) are therefore 0.02% and 0.01% respectively. Horizontal dimensions pertaining to scour profile measurements in the tests were measured using a measuring tape with the precision of 1 mm. This gives an estimated error for distance of maximum scour depth from nozzle (x_m) and distance of the maximum mound height from the nozzle (x_d) of 1% and 0.12% respectively. ASTM C670 has suggested a precision in sieve analysis of 3% for aggregates with nominal maximum size of 19 mm. Considering this precision range (3%) for D_{50}, an estimated error for derived parameter F_o can be 4.76%.

Table C-1: Maximum errors in measured and derived quantities

Quantity	Maximum error
b_o	0.04%
y_t	0.99%
y_t/b_o	1.03%
U_o	1.09%
F_r	1.13%
ε_m	0.02%
Δ	0.01%
x_m	1%
x_d	0.12%
D_{50}	3%
F_o	4.76%

The determination of uncertainty in the mean (u_m) and instantaneous (V) velocities measured by the LDA was carried out are based on the techniques developed by Moffat (1988) and Coleman and Steele (1999).

The uncertainty attributed to a measurement is an estimate of the possible residual error in that measurement after all proposed corrections have been made. The error or uncertainty is usually categorized as "fixed" or "random" and "bias" or "systematic". Random uncertainty depends on whether the error it introduces is steady or changes during the time of one complete experiment. It is also presumed to behave randomly, with a zero mean. It can be quantified by the following expression:

$$P_r^2 = \left[\sum_{k=1}^{M} (P_J)^2{}_k\right]^{\frac{1}{2}} \qquad \text{Eq. C-1}$$

where, P_J is equivalent to twice the standard deviation of the variable J, or a user-stated estimate of a repeatability error. Eq. C-1 sums the precision error for k sources of repeatability error and J number of variables. The bias in the measurement of a particular variable may be quantified in the following expression:

$$B_J = \left[\sum_{k=1}^{M} (B_J)^2{}_k\right]^{\frac{1}{2}} \qquad \text{Eq. C-2}$$

Eq. C-2 sums the systematic error of k elemental sources of bias and J number of variables.

To establish the total measurement error estimate (within a 95% confidence limit), the random and systematic uncertainties are combined using the root sum squared method:

$$U_r = \left(B_r^2 + P_r^2\right)^{\frac{1}{2}} \qquad \text{Eq. C-3}$$

The uncertainties in the mean (u_m) and instantaneous (V) velocities are thus estimated to be less than 1% and 2.5% respectively.

VITA AUCTORIS

Niranjan P Deshpande was born on 7th November 1977, in Mumbai, India. He graduated from the University of Mumbai, Mumbai, India, in June 2000 with a Bachelor of Engineering degree in Civil Engineering. He further acquired a Post Graduate Diploma in Civil Engineering from the University of Saskatchewan, Saskatoon, Canada, in December 2002.

He was accepted in the Faculty of Graduate Studies and Research at the University of Windsor, in 2003 leading to the degree of Master of Applied Science in Civil Engineering.